~~Trends~~ Seasonal to decadal variability and ~~seasonal signals in Atlantic feature-based~~ persistence properties of the Euro-Atlantic jet ~~stream characteristics and in weather types.~~streams characterized by complementary approaches

Hugo Banderier[1,2], Alexandre Tuel[3], Tim Woollings[4], and Olivia Martius[1,2,5]

[1]Institute of Geography, University of Bern, Bern, Switzerland
[2]Oeschger Center for Climate Change Research, University of Bern, Bern, Switzerland
[3]Galeio, Paris, France
[4]Atmospheric, Oceanic and Planetary Physics, University of Oxford, Oxford, United Kingdom
[5]Mobiliar Lab for Natural Risks, University of Bern, Bern, Switzerland

Correspondence: Hugo Banderier (hugo.banderier@unibe.ch)

Abstract. Recent studies have highlighted the link between upper-level jet stream dynamics, especially the persistence of certain jet configurations, and extreme summer weather in Europe. The weaker and more variable nature of the jets in summer makes it difficult to apply the tools developed to study them in winter, at least not without modifications. Here, to further investigate the link between jets and persistent summer weather, we present two complementary approaches to characterize the jet dynamics in the North Atlantic sector and use them primarily on the northern hemisphere summer circulation.

First, we apply the self-organizing map (SOM) clustering algorithm to create a 2D distance-preserving discrete feature space to the tropopause-level summer wind field over the North Atlantic. The dynamics of the tropopause-level summer wind can then be described by the time series of visited SOM clusters, in which a long stay in a given cluster relates to a persistent state and a ~~rapid~~ transition between clusters that are far apart relates to a sudden considerable shift in the configuration of upper-level flow.

Second, we adapt and apply a jet ~~axis~~ core detection and tracking algorithm to extract individual jets and classify them ~~in~~ intoto the canonical categories of eddy-driven and subtropical jets (EDJ and STJ, respectively). Then, we compute a wide range of jet indices on each jet for the entire year to provide easily interpretable scalar time series representing upper-tropospheric dynamics.

This work will ~~exclusively~~ focus on the characterization of historical trends, seasonal cycles, and ~~other statistical~~ persistence properties of the jet stream dynamics, while ongoing and future work will use the tools presented here and apply them to the study of connections between jet dynamics and extreme weather.

The SOM allows the identification of specific summer jet configurations, each one representative of a large number of days in historical time series, whose frequency or persistence had increased or decreased in the last decades. Detecting and categorizing jets adds a layer of interpretability and precision to previously and newly defined jet properties, allowing for a finer characterization of their trends and seasonal signals.

Detecting jets on ~~flattened pressure levels instead the 2PVU surface is more robust~~ pressure levels of maximum wind speed at each grid point instead of on the dynamical tropopause is more reliable in summer, and finding wind-direction-aligned subsets of 0-contours in a normal wind shear field is a fast and robust way to extract jet ~~features~~cores. Using the SOM, we ~~highlight a trend towards more negative NAO, and isolate predictable and/or~~ isolate persistent circulation patterns and assess if they occur more or less frequently over time. Using properties of the ~~jet features~~jets, we confirm that ~~jets get faster and narrower in winter, but not so clearly in summer, and~~ the northern hemisphere summer subtropical jet is weakening, that both jets get wavier, and that they overlap less frequently over time. We find no significant trend in jet latitude or in jet persistence. Finally, both ~~methods~~ approaches agree on a ~~sudden flow transition in~~ rapid shift in subtropical jet position between early and late June.

1 Introduction

Extratropical tropopause-level jet streams are narrow bands of westerly winds and are one of the most prominent features of the upper-tropospheric circulation. Their large variability at daily ~~timescales~~ time scale (Woollings et al., 2014) along with their link to extreme weather (e.g., Martius et al., 2006; Mahlstein et al., 2012; Harnik et al., 2014) makes them ~~a prime~~ an important object of research in meteorology and atmospheric dynamics.

From a climatological perspective, jet streams are often separated into two categories based on their location and momentum source (Kållberg et al., 2005; Koch et al., 2006; Harnik et al., 2014; Winters et al., 2020; Spensberger et al., 2023). The subtropical jet (STJ) is located at the poleward edge of the Hadley cell. It draws its momentum from the ~~thermally-driven~~ thermally driven Hadley cell circulation and is ~~mostly~~ mainly confined to high levels, typically between 400 and 150 hPa (Krishnamurti, 1961; Held and Hou, 1980). The eddy-driven jet (EDJ) can be found further poleward, inside the Ferrell cell. It is also referred to as the subpolar or extratropical jet. It is driven by momentum flux convergence associated with midlatitude synoptic eddies (Palmen and Newton, 1948; Held, 1975; Schneider, 1977; Woollings et al., 2010). It has a much deeper vertical extent, typically extending below 700 hPa. The separation into STJ and EDJ is not always clear, as both sources of momentum are often present to varying degrees to drive either jets and depend on each other (Lee and Kim, 2003; Martius, 2014).

Certain features and configurations of the jet have received particular attention over the last years due to their links to other aspects of the circulation, surface weather, or both. The latitude of the low-level EDJ has been identified as a major mode of variability of the wintertime Atlantic circulation (Athanasiadis et al., 2010; Woollings et al., 2010; Hannachi et al., 2012). A very zonal (low tilt) EDJ paired with a north-shifted STJ can create a rare but very persistent circulation pattern with a merged jet (Harnik et al., 2014). An instantaneously meandering jet is the marker of Rossby waves (e.g. Vallis, 2017), but strong narrow jets can act as waveguides for them too (Hoskins and Ambrizzi, 1993; Martius et al., 2010; Wirth, 2020; White, 2024). A locally sinuous jet may also mark the presence of a block (e.g. Nakamura and Huang, 2018; Woollings et al., 2018b). Jet properties also interact with each other. For instance, in winter, the EDJ's latitude influences its persistence and predictability (Franzke and Woollings, 2011; Barnes and Hartmann, 2011), and a jet with low speed has a higher daily variability in its waviness and latitude (Woollings et al., 2018a), which is hypothesized to ~~favorise~~ favor blocks. Jet ~~features~~ properties have also been linked to extreme events. The position of the EDJ modulates the odds of extreme events in the midlatitudes (Mahlstein et al., 2012),

and so does its waviness (Röthlisberger et al., 2016b; Jain and Flannigan, 2021). Over Eurasia, ~~a persistent double jet state~~ the persistent simultaneous presence of the EDJ and STJ is associated with increased odds of extreme heat in summer in certain regions of western Europe (Rousi et al., 2022). Recently, statistical models trained on timeseries of a few (5-10) wintertime EDJ properties (introduced by Barriopedro et al., 2022) were used to skillfully predict air stagnation (Maddison et al., 2023) and temperature extremes (García-Burgos et al., 2023).

Climate change is expected to affect the jet streams in several ways. Through connections highlighted in the previous paragraph, themselves potentially affected by climate change, trends in jet stream properties may translate into trends in various aspects of atmospheric circulation and surface weather (e.g. Held, 1993; Stendel et al., 2021). The poleward shift of the jet streams under climate change was hypothesised very early on (e.g. Held, 1993). It is now observed in historical data in the global mean, albeit more clearly in winter than in summer, and mostly for the EDJ. ~~The signal is however~~ However, the signal is weak in the North Atlantic sector (Woollings et al., 2023). This poleward shift is projected to continue in future simulations (Barnes and Polvani, 2013; Lachmy, 2022; Woollings et al., 2023). For the STJ, the historical trend is season- and region-dependent. For the North Atlantic sector, Totz et al. (2018) report a poleward trend in the transition seasons and an equatorward trend in summer. The North Atlantic STJ is also weakening with time, especially in summer (Woollings et al., 2023; D'Andrea et al., 2024), and so is the North Atlantic EDJ in the last two decades (Francis and Vavrus, 2012; Woollings et al., 2018a), although an opposite trend has been observed for longer time periods (Blackport and Fyfe, 2022). In future simulations, a positive trend is projected for the maximum speed of the EDJ core, although this signal is not yet apparent in historical data (Shaw and Miyawaki, 2024). In past data and using three different metrics, Francis and Vavrus (2015), Di Capua and Coumou (2016), and Martin (2021) all find slight increases in EDJ waviness, but a stable STJ waviness in the last cited paper. Further downstream however, Lin et al. (2024) find an increase in waviness for the Asian Jet that has an Atlantic origin. By contrast to past trends, for future winters, Peings et al. (2018) find a decrease in waviness accompanied by a strengthening and squeezing of the EDJ. This opposite trend in EDJ waviness for past and future data is consistent with the findings of Cattiaux et al. (2016), who find a slight increase in waviness in the past only for certain basins (including the North Atlantic) and seasons, but an overall decrease in waviness in future simulations. The conflicting results in jet meandering depending on the period and metric chosen were highlighted by Blackport and Screen (2020b) and overall remain a subject of discussion in the community (Geen et al., 2023).

Most of the current research in atmospheric science requires reducing the complexity of the circulation from time-varying 2D or 3D fields to a smaller feature space. These simplified feature spaces are either continuous, like jet indices (Woollings et al., 2010; Di Capua and Coumou, 2016; Barriopedro et al., 2022) or the projection of instantaneous fields on principal components, or discrete, like weather regimes (e.g., Michelangeli et al., 1995) or other types of clustering methods ~~(Weiland et al., 2021; Rousi et al., 2022)~~like the self-organizing map (Gibson et al., 2017; Weiland et al., 2021; Rousi et al., 2022; Stryhal . These methods can also be categorised based on the number of choices the user needs to make, from ~~data-driven, e.g. principal components, *k*-means, self-organizing maps,~~ statistical, e.g. dimensionality reduction or clustering, to expert-defined, e.g. jet indices, blocking indices ~~,~~ or wave breaking indices. ~~Data-driven~~ Statistical approaches are typically less fallible since they

require fewer choices, but tend to be harder to interpret than expert-defined features. ~~Data-driven~~ Certain statistical methods are also known to produce physically unrealistic patterns that can lead to wrong interpretations (Monahan and Fyfe, 2006).

~~In this work~~ Here, and to lay the groundwork for further research on all the interactions ~~previously cited~~between jet streams and other large-scale circulation features or surface weather events, we develop two complementary diagnostic tools for the jet streams. Using two methods allows us to view the circulation from different angles, and to combine the strengths of ~~data-driven~~ statistical and expert-defined approaches. Recently, Madonna et al. (2017) recommended the use of different, complementary, and problem-dependent approaches to describe the jet streams. Both of the diagnostic tools presented in this work are adaptations of existing techniques widely used in the field of atmospheric sciences, with implementation details changed and tailored for the specific needs of summertime, upper-level circulation.

The first one is ~~a clustering technique known as~~ the self-organizing map (SOM)~~. This data-driven clustering technique~~, a clustering algorithm. The SOM creates a distance-preserving discrete feature space that makes it a valuable tool to study ~~stationary~~ stationarity and recurrence (Tuel and Martius, 2023), a major factor in extreme events. The second one is a set of jet characteristics computed on individual jet ~~features~~ cores that are extracted, tracked, and categorized from wind fields. This provides a collection of continuous interpretable time series representing the jets over time.

After presenting both techniques in detail, we demonstrate their capabilities on reanalysis data. ~~The high-level objectives of the results presented in this work are to assess the seasonal cycle of the upper-level circulation through this new lens, find the trends, or lack thereof, in various metrics, and study to the circulation persistence under different aspects. This works focuses on summer, a season that~~ This work focuses more on summer than the rest of the year. This season receives less attention when designing methods to characterize the circulation, and is yet very important for extreme events and which presents interesting, different trends compared to the rest of the year (Harvey et al., 2023). The SOM will only be trained on June, July and August (JJA) days, but the jets are detected on year-round data to provide more context to the JJA results.

The seasonal varability of the upper level circulation is characterized using both the week-by-week mean pathway through the SOM and the seasonal cycle of the jet properties, and interannual trends are assessed for state occurence frequencies as well as for individual jet properties such as jet waviness. The SOM approach is related to the more established weather regimes, as their connections to weather impacts have been thoroughly studied. Finally, the persistence of the upper level flow, characterized using both state persistence using the SOM, and feature lifetime using jet tracking, is quantified. These preliminary results are in preparation for future work delving deeper into the comparison between these two, sometimes diverging, notions of persistence.

2 Data and Methods

2.1 Data

~~The European Centre for Medium-Range Weather Forecasts reanalysis version 5 (hereafter, ERA5 reanalysis; Hersbach et al., 2020) provides~~ We use 6-hourly gridded fields for the 1959-2022 period, over the 80 °W − 40 °E, 15 °N − 80 °N domain, extracted from the European Centre for Medium-Range Weather Forecasts reanalysis version 5 (hereafter, ERA5 reanalysis; Hersbach et al., 2020)

. The main variables we use are the horizontal wind components u and v, and the wind speed $U = \sqrt{u^2 + v^2}$, on ~~pressure levels ranging from 175 to~~ the six following pressure levels: 175, 200, 225, 250, 300 and 350 hPa.

Both algorithms take as input, at each timestep, ~~a single~~ 2D (longitude-latitude) ~~field~~ fields of upper-tropospheric wind. We flatten the three wind fields (u, v and U) in the vertical by retaining, at every grid point, their value at the pressure level where U is maximal since ~~the jets are the features that interest us~~our goal is to detect jet cores, and they are defined as local wind speed maxima. We keep track, in a separate 2D ~~array~~field, of that pressure level, to use later in the jet categorization. Both methods then add different preprocessing steps to this ~~flattened~~ vertical maxima data, which will be discussed in the relevant sections.

~~In addition to wind speedfields, we use~~ We additionally use the potential temperature on the surface of maximum wind speed, and the horizontal wind speed magnitude at the 500 hPa ~~geopoential~~ pressure level. Finally, summer Euro-Atlantic weather regimes (Cassou et al., 2005; Grams et al., 2017) are computed from 500 hPa geopotential height anomalies from ERA5, ~~and the daily North Atlantic Oscillation (NAO) index from the United States National Oceanic and Atmospheric Administration, computed following the method developed by Barnston and Livezey (1987) that provides a meaningful definition of NAO in all seasons~~computed relative to a daily climatology including all years from 1959 to 2022, smoothed with a 15-day centered rolling window.

2.2 SOM clustering

2.2.1 Definition

The self-organizing map (SOM) is a clustering method first introduced by Kohonen (1982) (see also Kohonen, 2013, for an in-depth review), whose main appeal over simpler predecessors like k-means is the creation of a 2D distance-preserving discrete feature space. The SOM may be presented as a modification of k-means. In k-means, data points are split in k groups called clusters, such that the variance within the clusters is minimal and the variance between clusters is maximal. Each cluster is then represented by the mean of all its members, called the cluster center or sometimes weights matrix. The SOM adds another layer to this algorithm, by ~~arraying~~ placing the clusters on the nodes of a regular 2D grid of size $k = n \times m$, typically rectangular or hexagonal, ~~based on~~ and has a distance metric ~~and a neighborhood function~~on this discrete space, for example the Euclidean distance between nodes. There, a cluster i is defined by its weights matrix $\mathbf{w}_i$ which is not equal in general to its center, but rather the result of a training process during which clusters on neighboring nodes have an influence modulated by the distance between nodes. Hereafter, we conflate the clusters and the nodes they sit on, and the phrases "distance between clusters" and "neighboring clusters" are to be understood as, respectively, "distance between the nodes on which the clusters sit" and "clusters on neighboring nodes".

The training then has a similar objective as k-means, with the additional constraint that a pair of neighboring clusters should be more similar to each other than a pair of distant clusters. This constraint ensures the distance-preserving property of the created phase space. The desired similarity of neighboring clusters may be enforced by the choice of an appropriate neighborhood function. The neighborhood function, typically a Gaussian~~function of the~~ , is a parametric function with parameter σ,

the neighborhood radius, and is applied to the distance between clusters in the training process. The convergence ~~is helped by a scale parameter~~of the algorithm relies on decreasing σ~~that slowly decreases during training, but the decay function and the initial~~ , equivalent in our case to the Gaussian's scale parameter, over time during the training. However, the initial and final σ ~~value~~ values as well as the decay function are additional choices that need to be made. In general, a larger σ allows for more similar ~~neighbors~~neighbours, and the limiting case $\sigma \to 0$ is equivalent to k-means.

Both the SOM and k-means share the same challenge, that is the choice of the number of clusters k. The SOM further adds the choice of the shape of the grid, $k = n \times m$.

Allowing neighboring clusters to be similar ~~inevitably leads~~ can lead the SOM to be a ~~strictly~~ worse clustering algorithm, in the usual sense of cluster separation, than k-means~~. It should only be used if one needs~~ , if the neighborhood radius is different from zero at the end of training (Gibson et al., 2017). Its strength resides in the creation of a distance-preserving feature space.

One of the reasons we use SOM is the interpretability of the ~~projected trajectory~~ trajectory when expressed as a succession of cluster visits. Once the SOM is trained, each timestep ~~belongs~~ is assigned to a cluster, its "best matching unit" or BMU, defined as $\mathrm{BMU}(t) = \mathrm{argmin}_i \|\mathbf{x}_t - \mathbf{w}_i\|$ with $\mathbf{x}_t$ the wind field at timestep t. Thus, the input time series is represented as a succession of *stays* in clusters and *jumps* between clusters, where long *stays* or short *jumps* point to persistence, and long *jumps* indicate abrupt changes in the configuration of the upper-level flow.

2.2.2 Specific implementation

For the SOM algorithm, the ~~flattened JJA~~June-July-August (JJA) vertically maximum wind speed field (see Data) is coarsened to a $1.5°$ resolution grid to reduce the computational complexity and to focus on the larger scale features. However, the final results are shown at the initial $0.5°$ resolution. This is done by representing clusters with their centers, computed with the original higher resolution data, rather than their weights.

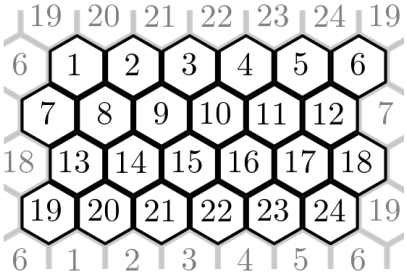

Figure 1. Hexagonal topology SOM with ideal grid size. The SOM clusters are in black and the grayed clusters illustrate the periodic boundaries.

The grid (of size $n \times m$) is hexagonal with periodic boundary conditions, and is associated with a discrete distance metric. ~~All~~ As a consequence, clusters are at a unit distance away from their nearest neighbors, and the bottom row and left column ~~also~~ are at a unit distance away from the top row and right column, respectively (see figure 1)~~. In order to~~ , such that each and

every cluster has six neighbors, all at a unit distance. Periodic boundary conditions were chosen to avoid creating an artificial over representation of the central clusters, which would have diminished the relevance of our persistence measures later on. The SOM is initialized using the first two principal components of the input data to ensure reproducibility, as recommended in Kohonen (2013). Before training, the data is standardized and weighted by the cosine of latitude. We use the single batch training algorithm (Kohonen, 2013), repeated 50 times with the neighborhood radius σ exponentially decaying from 2 to 0.2. This training algorithm does not involve a learning rate.

To inform our decision on the SOM grid size, we use two performance metrics of the SOM. The first one is the energy function E of the SOM based on Heskes (1999) (see eq. 1), and the second one is the 5$^{\text{th}}$ percentile of the projection of data points on their BMUs, defined as P in eq. 2. These metrics are a function of the ensemble of SOM weights $W = \{\mathbf{w}_i, 1 \leq i \leq n \times m\}$, the ensemble of input data vectors $\mathbf{x} \in X$, of size N, as well as the topological properties of the SOM. The grid distance between two SOM clusters i and j is precomputed and stored in a ~~matric~~ matrix of elements d_{ij}. These distances are then transformed by the neighborhood function to obtain the pairwise neighborhood parameters $h_{ij} = f(d_{ij}; \sigma)$ based on the SOM's ~~scale parameter~~ neighborhood radius σ. In this work, f is a zero-mean Gaussian with scale parameter σ.

$$E(W) = \frac{1}{N} \sum_{\mathbf{x} \in X} \min_{1 \leq i \leq n \times m} \sum_{j=1}^{n \times m} h_{ij} \|\mathbf{x} - \mathbf{w}_j\|^2 \tag{1}$$

$$P(W) = \underset{\mathbf{x} \in X}{Q_5} \left(\max_{1 \leq i \leq n \times m} \frac{\mathbf{x} \cdot \mathbf{w}_i}{\|\mathbf{x}\| \|\mathbf{w}_i\|} \right) \tag{2}$$

The goal is to minimize E and maximize P while maintaining a reasonably low number of clusters. The E and P objectives are similar, but the latter allows one to explicitly limit how poor the poorest projections on the SOM clusters are, making sure that most days are well-described in the 2D feature space described by the SOM since current and future work includes working on extreme configurations of the upper-level circulation. Testing for many sizes ranging from 4×4 to 9×9 was performed, and the chosen size is 6×4.

2.2.3 SOM metrics

We compute statistical properties from the trained SOM, including the populations of each cluster and their annual trends, two quality metrics as well as the average and maximum residence time in a given cluster~~, and the transition probability matrices at various time lags. Formally, from an integer time series of BMUs $\mathrm{BMU}(t)$, the transition matrix at lag ν (integer number of timesteps forward) M^ν has elements $M^\nu_{ij} = \mathbb{P}(\mathrm{BMU}(t+\nu) = j | \mathrm{BMU}(t) = i)$~~.

The ~~transition matrices allow, among other things, to compute a SOM metric that a SOM metric that characterizes immediates predictability in the spririt of the local dimension in dynamical systems theory. Local dimension is a metric that measures, for every point along a high-dimensional trajectory, the amount of active degrees of freedom (see e.g. Faranda et al., 2017) . Our predictability metric is named dilution and is defined for each cluster j and lag ν as $\sum_i M^\nu_{ij} d_{ij}$. This corresponds to the expected value of d_{ij}, given the discrete probability distribution (for a given cluster j) M^ν_{ij}. It informs on how long the SOM-space trajectories leading to cluster i typically are.~~

~~The second SOM metric of~~ first SOM metric of note is an ~~equivalent~~ analogue to the persistence index in dynamical systems theory. The average ~~(resp. maximum)~~ residence time at a given cluster i is simply given by the average ~~(resp. maximum)~~ length of time during which $\mathrm{BMU}(t) = i$, starting at the transition from another cluster to i. The definition can be loosened to the length of time during which $\mathrm{BMU}(t)$ ~~stays~~ remains within a given distance of i. With a large SOM~~with sometimes~~, that sometimes features minute differences between neighboring clusters, this second definition with a small distance ~~of 1 or 2~~ can be a more realistic measure of persistence. ~~Here, we use a value of 1, meaning a residence on cluster i continueswhile the trajectory stays on cluster~~ To account for varying degrees of similarity between neighboring clusters, we do not use the discrete grid distance between clusters but instead the Euclidean distance between SOM cluster weight matrices. At the start of JJA, the first stay starts on the first populated cluster, i_0. As long as $\mathrm{BMU}(t)$ is on i_0 or any other cluster whose weight matrix is at a low enough distance from that of i_0, with as threshold the 10^{th} percentile of inter-cluster-weight distances, the stay continues. The first timestep $\mathrm{BMU}(t)$ stops respecting this condition to arrive at another cluster i_1, a new stay starts with the same condition for it to terminate. The stay is associated to the most visited cluster during the stay, which is not necessarily the starting one.

We provide two cluster-wise quality metrics. The first one is the root mean square error (RMSE), defined for each cluster as the mean Euclidean distance between its weight matrix and its members. A low RMSE is preferred. The second quality metric is the cluster separatedness. We compute, for each pair of clusters, the ratio of the Euclidean distances between their weight matrix to the grid distance that separates them. We then average all the ratios for all the pairs containing cluster i ~~or any of its six direct neighbors.~~ to obtain cluster i's separatedness. A high separatedness is preferred.

Finally, we will relate our SOM clustering to the summer Euro-Atlantic weather regimes. Following Grams et al. (2017) but using only for four weather regimes, we assign to each day of summer one of four weather regimes if the associated weather regime index is bigger than that of the three other regimes for at least 5 consecutive days and is above its temporal standard deviation within this time span. With this definition, 40 % of the timesteps are not assigned to any weather regime. We then count the number of timesteps previously assigned to a SOM cluster that are now also assigned to a weather regime.

2.3 Feature detection and tracking

The SOM is a powerful ~~data-driven~~ clustering tool to characterize the circulation as a whole in a given region. However, one might want to know more specific information about some of the components of the circulation, expressed as numbers rather than features on a composite map. We now turn to the methods we use to detect jets in ~~flattened~~ vertical maximum 2D wind fields, to separate them into broad categories, to track them over time to assess their lifetime and evolution, and finally to extract a wide range of properties out of them. Thanks to seasonally-varying thresholds (see next section), our method works equally well across the year. ~~This is why~~ Therefore, we apply it to the full dataset rather than only to ~~summer~~JJA, which will allow us to broaden the discussion of inter-annual trends to other seasons and paint a full picture of the ~~summer~~ jets' annual cycles.

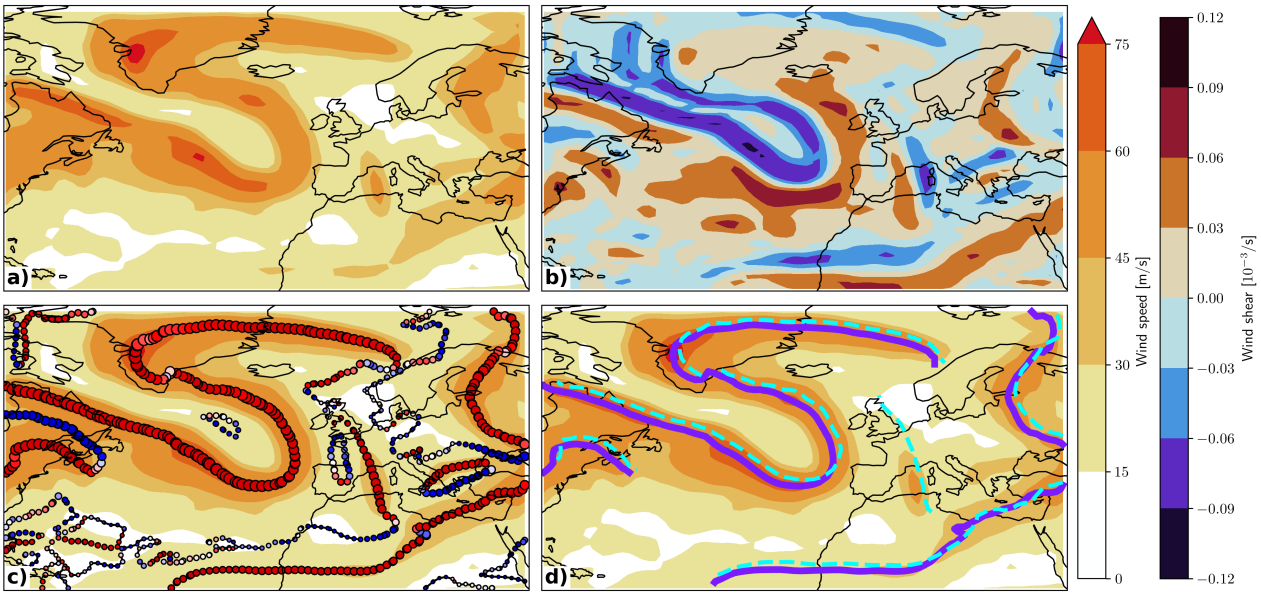

Figure 2. Results of our jet detection algorithm for 0000 UTC 9 Oct 1959. a) The smoothed, ~~flattened~~ vertical maximum wind speed [m/s] field given as input to the algorithm. b) The smoothed horizontal normal wind shear on the same ~~flattened~~ 2D surface. c) The $\tau = 0$ contours where the size of the points corresponds to the wind speed field, and the color corresponds to the alignment with the horizontal wind vector field from blue (close to -1) to red (close to $+1$). d) The jets extracted from contours, as solid purple lines. The output of the S17 algorithm is represented as dashed cyan lines for comparison.

2.3.1 Jet detection

Our jet detection algorithm is an ~~updated~~ adapted version of the method by Spensberger et al. (2017, hereafter S17). It can be applied to each timestep independently, allowing for parallelization. ~~As for the SOM, the flattened wind~~

The vertical maximum wind speed fields (u, v and U; see Data) are coarsened to a grid of $1.5°$. ~~As a first difference to S17, we use vertical maxima over several high-altitude pressure levelsinstead of the 2PVU surface~~Our choice of 2D fields, the level of maximum wind speed over several pressure levels, as described in Data, is the first difference to S17, who used wind fields interpolated onto the 2 PVU surface, where 1 PVU = $10^{-6}\mathrm{Kkg^{-1}m^2s^{-1}}$. Internal testing has shown that the STJ is often undetectable on the ~~2PVU surface in summer~~2 PVU surface in JJA, while it clearly appears on our ~~flattened~~ 2D fields. The main criterion used to find jets is the horizontal normal wind shear $\tau := \frac{\partial U}{\partial n} = \frac{v}{U}\frac{\partial U}{\partial x} - \frac{u}{U}\frac{\partial U}{\partial y}$. Following Berry et al. (2007), $\tau = 0$ is a necessary condition for a jet. The first step of this algorithm is thus to find ~~smooth~~ contours of $\tau = 0$~~. First, a Fourier transform is applied to the τ field in the longitude (λ) and latitude (ϕ) directions, yielding $\tilde{\tau}$ defined on a 2D space of Fourier coefficients (k_λ, k_ϕ). This function is truncated following $|k_\lambda + k_\phi| > K \implies \tilde{\tau}(k_\lambda, k_\phi) = 0$ with $K = 0.3 \times n_\lambda \times n_\phi$ before applying an inverse Fourier transform on the truncated Fourier field. Then, a contour library is applied to extract contours of $\tau = 0$ as lists of (λ, ϕ) coordinate pairs~~using a contour detection routine.

~~Jets are then extracted as subsets of these contours , using~~ The points along the contours are filtered using a wind speed and ~~alignment criteria for each point of the contour. First, the wind speed must be high enough for a grid-point to be considered a part of a potential jet.~~ an alignment threshold. We use as wind speed threshold the day-of-year climatological 75$^{\text{th}}$ percentile of 6-hourly wind speed, so that the algorithm works equally well in all seasons. ~~Second, the contour must~~ The contour must also be aligned with the wind speed. This is done by computing the local tangent vector $\mathbf{t} = \frac{\mathrm{d}\mathbf{x}}{\mathrm{d}s}$, with s the linear path coordinate, and computing the alignment dot product $a = \frac{\mathbf{t}}{\|\mathbf{t}\|} \cdot \frac{\mathbf{u}}{U}$, as done in Molnos et al. (2017). We require $a > 0.3$ for a jet. With very few values of a different from either -1 or $+1$, the performance of the algorithm is largely insensitive to the exact value of this threshold.

~~Finally, jets~~ Jets are defined as ~~the longest~~ series of consecutive ~~points that follow these two criteria, allowing for~~ potential jet points, i.e. points in the contours that follow the two point-wise criteria defined in the previous paragraph. We allow series to contain small stretches of ~~1 to 3~~ one to three points that do not respect ~~them in between. The jets themselves~~ the thresholds if they are surrounded by points that do. The series need to verify ~~two criteria to be considered as such. First, the~~ one additional criterion to be finally accepted as jets. The path integral of the wind speed along ~~their cores needs to be above a day-of-year varying threshold, and the average of all their local alignment dot products needs to be above 0.6~~the path of the series is computed using a method detailed in section 2.3.2 and is compared against a day-of-year-varying threshold, heuristically constructed from the wind speed threshold U^*, the radius of the Earth R, the longitudinal extend of the domain $\Delta\Lambda$ as $U^* R \Delta\Lambda \cos(45°)/3$.

Each jet J_a of length L_a is represented as a sequence of L_a points $k = 1 \dots L_a$, themselves a collection of coordinates with longitude λ_a^k, latitude ϕ_a^k, pressure p_a^k level, along with additional point-wise properties that can be of use to derive jet properties, e.g. the u_a^k or v_a^k components of wind or the wind speed U_a^k.

Figure 2 demonstrates the jet detection algorithm in four steps and compares its results against the original S17 algorithm~~.~~ ~~Our algorithm has very comparable results to~~ , but applied to the same 2D data to ignore the potential problems raised by the 2 PVU surface in this basin. The algorithms produce similar results with a few disagreements that can be explained by studying the differences between our algorithm and S17. ~~The two difference, finding~~ Our algorithm finds 0-contours of τ rather than low values of $\frac{\mathrm{d}\tau U}{\mathrm{d}n}$ ~~, and extracting~~ $\frac{\mathrm{d}(\tau U)}{\mathrm{d}n}$, extracts jets as subsets of contours using an alignment criteria instead of connecting points using a shortest-path algorithm~~,~~. These two differences seem to help find jet cores closer to the local wind maxima, a problem that was highlighted in the original work. Furthermore, by allowing jets to not respect the two local criteria (speed and alignment) for up to three points, our algorithm is more likely to find one long jet rather than several shorter pieces. This latter point is sometimes a problem when an EDJ and a STJ are detected as one long single jet. However, this does not happen often in 6-hourly data, and it is typically accompanied by ~~a sudden~~ an abrupt change in pressure level, wind speed, or alignment along the jet core, which helps to highlight and resolve these cases. This issue is not solved systematically in the current version of the algorithm, but might come in a later version.

2.3.2 Jet properties

Introduced by Woollings et al. (2010), the Jet Latitude Index (JLI) measures the latitude of maximum wind speed in the profile obtained by averaging the wind speed field at low altitudes, to filter out the STJ and only capture the EDJ, in a longitudinal band, originally $60\,°\mathrm{W} - 0\,°\mathrm{E}$, the North Atlantic basin. It is often used in combination with the Jet Speed Index (JSI), the maximum wind speed used to find the JLI. These simple and highly interpretable metrics have been used to describe ~~jet stream~~ EDJ variability at timescales ranging from daily to multi-decadal (Woollings et al., 2014, 2018a).

Over time, several other similarly simple yet powerful jet indices have been developed to describe the jet stream in a simplified way, or to link it to other phenomena. Such indices include the zonal jet index (Harnik et al., 2014), several sinuosity/waviness metrics ~~(Francis and Vavrus, 2015; Di Capua and Coumou, 2016; Cattiaux et al., 2016; Röthlisberger et al., 2016a)~~ (Francis and Vavr linked to extreme events and persistence (Röthlisberger et al., 2016b; Martin and Norton, 2023), up to a ten-index toolbox (Barriopedro et al., 2022) that has been used for skillful predictions of cold and hot spells in Europe (Maddison et al., 2023).

In the presence of several jets, many of these indices give an incomplete or improper picture. Using our ~~feature~~ jet core detection algorithm (section 2.3.1), all the jet indices can be computed for each jet ~~object~~ individually. The details of computations and potential differences with the original metrics are explained in the following paragraphs.

In the previous section 2.3.1 we mentioned point-wise jet properties storing each point's position and wind speed. The mean of these point-wise jet properties constitute the first jet properties we compute. The ones of interest correspond to the mean position of the jet. The properties `mean_lon`, `mean_lat` and `mean_lev` are all computed as weighted averages of the longitude λ, the latitude ϕ and the pressure level p respectively, using the point-wise wind speed values U_a^k as weights. In the spirit of the JLI, the maximum wind speed is found and stored as `spe_star`. The position on the (lon-lat) plane of this maximum is stored as `lon_star` and `lat_star`.

A path integral of the wind speed along the jet core and using the haversine distance is performed and stored as `jet_int`. Explicitly, the integral $\int U \mathrm{d}s$ is discretized using central finite differences and computed with a discretized approximation of

$$\mathrm{d}s = 2R \arcsin \sqrt{\sin^2\left(\frac{\mathrm{d}\phi}{2}\right) \cdot \cos^2\left(\frac{\mathrm{d}\lambda}{2}\right) + \cos^2(\phi) \cdot \sin^2\left(\frac{\mathrm{d}\lambda}{2}\right)}$$

with $R = 6.378 \times 10^6\,\mathrm{m}$ the radius of the Earth. This integral is performed once more over a smaller domain ($\lambda > 10\,°\mathrm{W}$) and stored as `int_over_europe`.

To obtain the local width of the jet a at a point k along its core, normal segments are drawn in continuous space on either side of the jet core, of length $10°$ each. Along each segment, the wind speed is interpolated from the gridded wind speed field. For each segment, the haversine distance between the core and the first point to have a wind speed below ~~$0.5 \times U_a^k$~~ $0.75 \times U_a^k$ represents the local width of the jet on this side, and the full local width is the sum of the local widths computed on either side. In some cases, only one segment can be drawn if the jet core is too close to a boundary. In this case, the local width is simply twice the width computed on the only valid side. The local widths w_a^k are computed ~~only every 5 jet core points to make the computations faster~~on every jet core point, and then averaged, with U_a^k as weights, to finally obtain the jet's mean `width`.

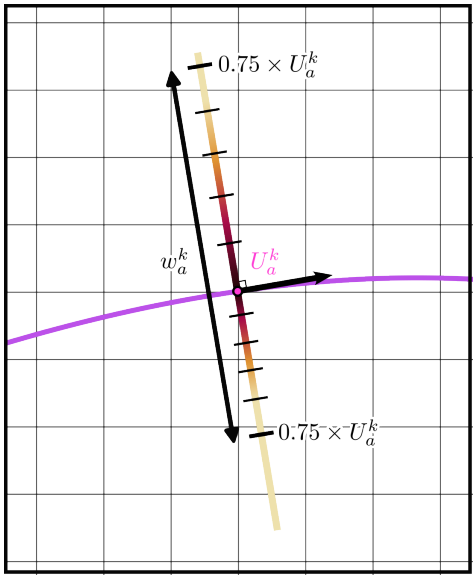

Figure 3. Schematic representing the local width computation, along a jet core a drawn in purple, for a single point k. In the schematic, the wind speed interpolated onto the half-segments is represented using a color gradient from black (core wind speed at the point of interest, U_a^k) to yellow (~~half~~ three quarters of local jet core wind speed, ~~$0.5 \times U_a^k$~~ $0.75 \times U_a^k$) with a tick every ~~$0.1 \times U_a^k$~~ $0.05 \times U_a^k$. The schematic, especially the grid spacing, is not to scale.

The tilt of the jet is computed as the slope of a U_a^k-weighted linear fit of the ϕ_a^k against the λ_a^k. The linear coefficient is stored as `tilt`, while the intercept is discarded. The quality of this linear fit, the R^2 value, is used to compute a natural measure of jet waviness: `waviness1` $= 1 - R^2$. Another natural way of characterizing waviness from jet ~~objects~~ cores is the U_a^k-weighted average distance between ϕ_a^k and `mean_lat`, stored as `waviness2`. For short jets, the difference between the tilt and the waviness is hard to assess, and in this case `waviness1` will not capture waviness well. However, if a jet is both tilted and wavy, only `waviness1` will be able to separate these properties. These two waviness metrics are compared against adaptations of waviness metrics found in the recent literature. `wavinessFV15`, adapted from Francis and Vavrus (2015), is computed as the U_a^k-weighted average of the local meridional circulation index: $\mathrm{MCI}_a^k = \frac{(v_a^k - \overline{v_a})|v_a^k|}{(U_a^k)^2}$. `wavinessDC16`, adapted from Di Capua and Coumou (2016), is computed as the ratio between the haversine-integrated length of the jet ($\int 1 \mathrm{d}s$) to the length of the circle arc $\overline{\phi} \cdot R \cdot \Delta\lambda_a$, where $\overline{\phi}$ is `mean_lat` and $\Delta\lambda_a$ is the extent of the jet in longitude expressed in radians. Finally, `wavinessR16`, adapted from Röthlisberger et al. (2016a), is computed as the sum of absolute differences in latitudes between neighbors $|\phi_a^{k+1} - \phi_a^k|$, divided by the sum of differences in longitudes.

An index that can be computed that will not be categorized per jet is the double jet index. From the found jets, a 2D (time-lon) binary array is built, where an element is set to `True` if at least 2 jets can be found at this timestep and longitudinal band over all latitudes and one hemisphere. The index is the zonal average of this array for longitudes over Europe, $10\ ^\circ\mathrm{W} < \lambda < 40\ ^\circ\mathrm{E}$.

In section 2.3.4, tracking the jets allows ~~one to add to this list~~ us to determine the lifetime of ~~the jet~~ a jet object, as well as the instantaneous speed of the jet's center of mass.

2.3.3 Jet categorization

While some literature sees the types of jets highlighted in the introduction as regimes of a singular jet stream (Harnik et al., 2014, 2016), this ~~framework~~ work benefits from seeing them as categories one may assign to the previously detected jets. In instantaneous data, one cannot distinguish the jet from the eddies potentially driving it, since the quantification of the eddy momentum flux requires temporal filtering and averaging (e.g. Lachmy, 2022). One ~~instead has to rely on depth~~may instead rely on the vertical extent or baroclinicity of the jet, which is sometimes misleading due to the many factors influencing low-level winds, latitude, which is not sufficient on its own for global data (Winters and Martin, 2017), or potentially other metrics like ~~shear (Martius et al., 2010)~~vertical shear (Martius et al., 2010) or the height of the tropopause above the jet core. A recent, promising approach to establish this categorization bins ~~and counts~~ the jets on the 2D feature space (Wind speed — Potential Temperature). The algorithm then extracts regions of high occurrences for oceanic basins across the world and for ~~both winter and summer~~the whole year. The approach always finds two distinct regions that may be labeled STJ and EDJ, except for the North Atlantic basin in ~~summer (Spensberger et al., 2023, see supplementary material for summer).~~ JJA (Spensberger et al., 2023, see their supplementary material for JJA).

A very similar approach is used here~~. It~~ , but with another feature space to better highlight the weak but still present bimodality in jet property distribution in this basin and season. Our version of the algorithm uses the (~~Mean latitude — Mean longitude — Pressure level) 3D~~ baroclinicity – potential temperature) 2D phase space and fits a two-component Gaussian Mixture model to facilitate the discovery of the two regions. The ~~model is~~ baroclinicity or vertical extent proxy is similar to that used by Koch et al. (2006), and is defined as the ratio of low level (500 hPa) horizontal wind speed magnitude at the horizontal position of the jet point and the jet core speed itself. The illustration of this binning can be seen on figure 4, where the count of each hexagonal bin is represented by its lightness and size.

A two-component Gaussian mixture model assumes that the data are bimodal and tries to fit their empirical distribution as a sum of two Gaussian distributions. Each Gaussian is defined by its mean and covariance matrix, and these are the parameters the model fits to the data. The model is fitted independently for each ~~season~~ month to accommodate the large seasonal variation in the STJ's ~~mean latitude. Each binned point in the histogram corresponds to a whole jet instead of the jet points used in the original paper.~~

~~The demonstration of the jet categorization can be seen on figure 4. Aside from expected results, it shows that the spatial density overlap of the two jets, a potential sign of misdetected jets , is seen mostly over North Africa in winter and is quite low. When studied in more details, most of this spatial overlap is physically sound, as it corresponds to jets of different mean pressure levels, the third dimension of the criterion used, and depths, characterzied using wind speed at low altitude pressure levels (not shown)~~occurence frequency. The density in the EDJ Gaussian component at each point, computed using the standardized distance to this component's center, is then used as a continuous score and not a hard assignment. The EDJ component is identified as the component with lower potential temperature. Most jet points will have a score close to 0 (STJ

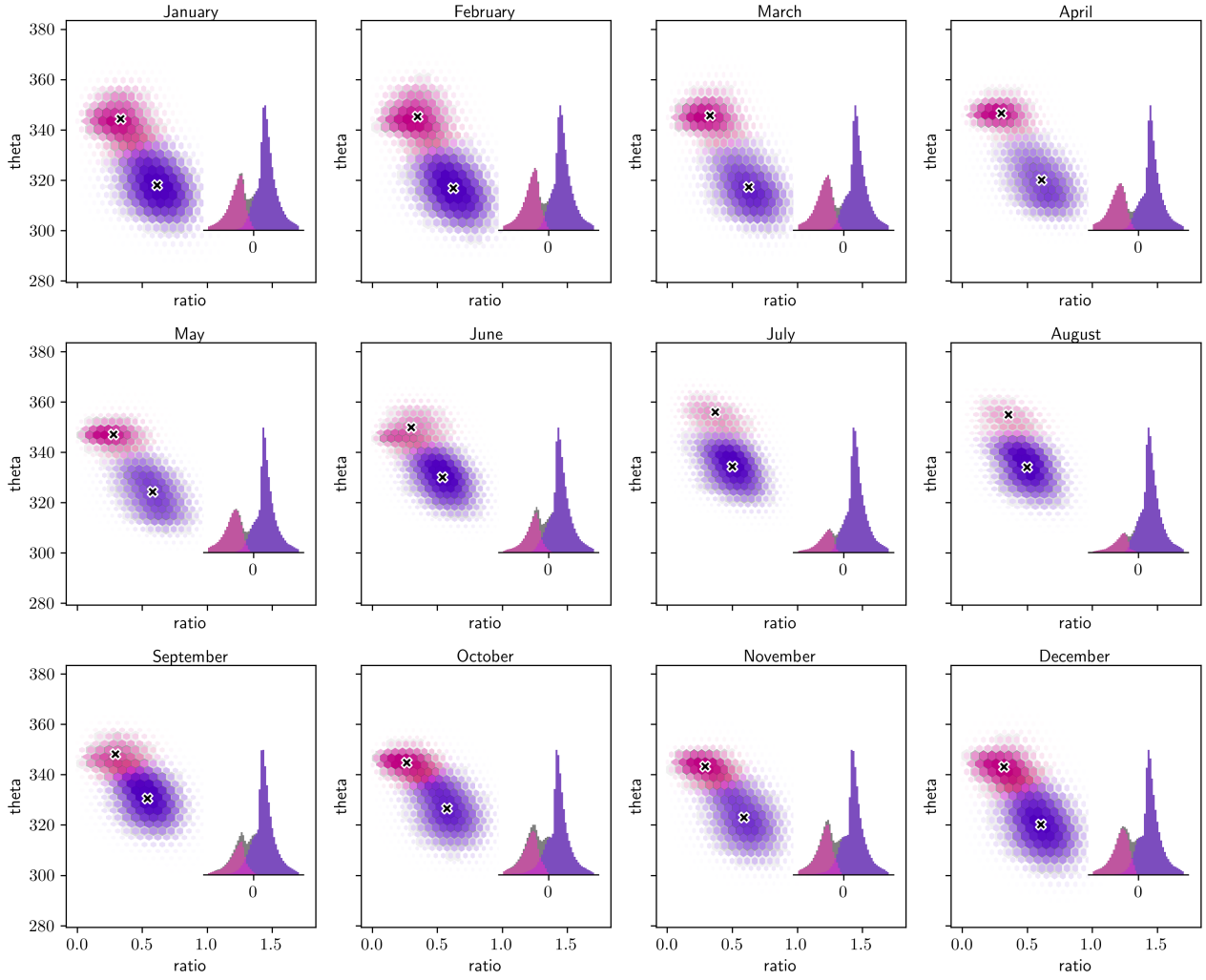

Figure 4. Demonstration of the jet categorization ~~. a, b) For~~ for each ~~season, here JJA,~~ month of the ~~jets~~ year. The jet points are ~~arrayed on~~ binned in the ~~3D phase~~ 2D space (~~Mean latitude~~ baroclinicity proxy — ~~Mean longitude — Pressure level~~potential temperature)~~and binned hexagonally. The lightness represents the density of jets in each bin~~, in ~~arbitrary units. A two-component Gaussian Mixture model is fitted~~ order to illustrate the ~~projected data,~~ underlying distribution in this 2D space. The size and ~~the labels~~ lightness of each ~~bin are averaged and represented as a~~ hexagon illustrate its height, while its color ~~ranging~~ indicates the mean Gaussian assignment score, from pink ~~for the~~ (0 score, close to STJ component) to purple ~~for~~ (1 score, close to EDJ ~~. c-f~~component)~~Spatial density~~ . The crosses indicate the center of ~~detected jets in arbitrary units~~each Gaussian, ~~colored by categories: pink for STJ~~ x_1 and ~~purple for EDJ for all four seasons~~x_2. On the lower right corner of each box, the quantity $\log \frac{\|x-x_1\|}{\|x-x_2\|}$ is binned, where x is a 2D vector containing a jet point's vertical extend proxy and potential temperature, and $\|y\|$ is the 2-norm of the vector y. This quantity is not the final score but serves illustrative purposes. The ~~latter four panels have~~ final score is averaged for each bin and indicated with the ~~same arbitrary scale~~color of each bar, as for the hexagons.

point) or close to 1 (EDJ point), but some points lie inbetween and can be thought of as hybrid. The jets as a whole are assigned a category based on the mean of the scores of the points that constitute them. Again, while most of the jets have a mean score close to either 0 or 1, some lie inbetween and can be thought of as hybrid.

The nature of this potential hybrid jet category is discussed in Appendix A. In short, it has an almost identical seasonal cycle to that of the STJ and is almost only present in JJA. Our final decision was therefore to carry on with only two categories, with a categorization cutoff informed by the distribution of EDJ component mean score.

2.3.4 Jet tracking

A straightforward ~~feature tracking~~ object tracking algorithm is presented in this section. The program will assign a flag n to each jet at each timesteps, where the flag is carried over from a jet in a timestep to a jet in the next one according to a distance threshold.

The algorithm starts by assigning each jet in the first timestep a unique flag $1, 2, 3 \ldots$. It then iterates over all timesteps t. For all flags that have appeared at least once in the previous four timesteps ($t-1$, $t-2$, $t-3$, $t-4$, i.e. a day with a time resolution of 6 hours), the algorithm extracts the most recent jet with this flag into a list of potential parents. This allows for jets to disappear for a few timesteps and mitigates the issue of short jets blinking in and out of the jet integral threshold from section 2.3.1. The potential children are all the jets present in the current timestep. For all pair of a potential parent jet a and a child jet b, an overlap measure $o_{a,b}$ as well as a vertical distance $\delta_{a,b}$ are computed as described in equations 3 and 4.

$$o_{a,b} = \frac{|\Lambda_a \cap \Lambda_b|}{2} \left(\frac{1}{L_a} + \frac{1}{L_b} \right) \tag{3}$$

$$\delta_{a,b} = \frac{1}{|\Lambda_a \cap \Lambda_b|} \sum_{k,l:\lambda_k=\lambda_l}^{L_a,L_b} |\phi_l - \phi_l| \tag{4}$$

Where Λ_a is the ensemble of longitudes in jet a.

Both overlap and vertical distance metrics need to satisfy a certain threshold, respectively 0.5 and 10°. If both are met, the jets match and the child jet is assigned the parent's flag. If a child matches no potential parent, it is assigned a new flag, the latest assigned flag plus one. If a child has two potential parents fulfilling both criteria, or if a parent has two children fulfilling them, the winner is the most recent one, and if both are as recent then it is the longest. ~~If the algorithm works on only a portion of the year, the flags are reset at the beginning of each year.~~

Using this, it is possible to infer the lifetime of a jet from its genesis to its decay, as well as to track the speed of its center of mass (COM), in $\mathrm{m/s}$ using the haversine distance between two ~~6H timesteps~~6-hourly timesteps. The first use of these new jet properties is to filter out jets with 1- or 2-timestep lifetimes to filter out residual noise. The lifetime and (the inverse of the) COM speed can be seen as additional measures of persistence of the ~~circulation~~ jet and can be compared against those developed within the framework of the SOM.

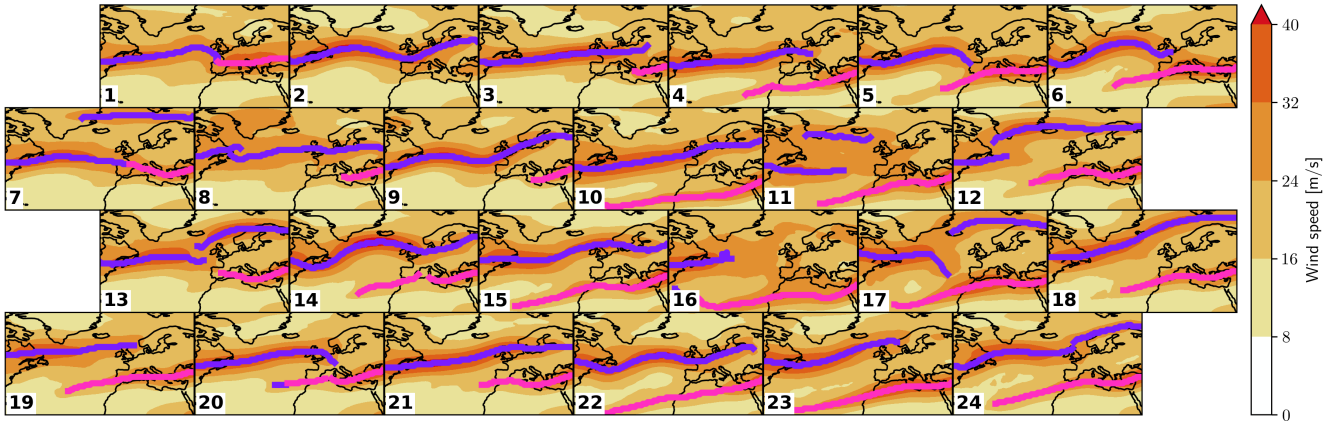

Figure 5. SOM training results on ~~summer~~ JJA wind speed fields. Composites of horizontal wind speed for all days corresponding to a cluster, and result of the jet core detection algorithm applied to the composite wind fields overlayed as colored lines; pink for STJ and purple for EDJ. The SOM cluster number is indicated by a number in the bottom left corner.

3 Results

3.1 ~~JJA~~ Atlantic ~~Jet~~ JJA SOM space

The ~~result~~ results of the SOM training are summarized in figure 5 ~~on the discrete phase space created by the SOM~~ in a grid that represents its topology. Each panel is a ~~composite of the wind fields of~~ wind speed composite of all timesteps belonging to the corresponding cluster. The population of each cluster is shown in Figure ~~??~~6a). The jet finding and categorization algorithm is applied to these composites, and the results are overlaid with purple and pink lines for the extratropical and STJs, respectively. Since composites have lower wind speeds than instantaneous data, the point-wise wind speed threshold is lowered to $20\,\mathrm{m.s^{-1}}$ and the jet-wise integrated wind speed threshold to $3 \times 10^8\,\mathrm{m^2.s^{-1}}$. Long jets that exhibit a EDJ region and a STJ region (see section 2.3.1) are split into two automatically, on clusters 1 and 7, so that we can later on derive jet properties directly from the SOM composites, in Appendix C.

~~The SOM is used with a high number of clusters (24) . This is much more than, for example, the canonical four summer weather regimes (Michelangeli et al., 1995; Grams et al., 2017). It allows for a finer separation of timesteps but leads to cluster pairs that look similar at first glance. The interpretation of the SOM can however be simplified, if necessary, by looking at groups of a few clusters at a time, or regions of the phase that exhibit a feature of particular interest . Some of these regions are highlighted here for future reference. It is worth reminding that the boundaries of the SOM space are periodic, meaning that opposite edges form a contiguous region. The high-zonal-overlap double jet states occur on the center-left side , as will be later confirmed when looking at the aggregated jet properties. This region consists of long, south-shifted STJs and large zonal overlaps of the STJ and the EDJ, while~~ We first assess a few regions of interest in the SOM from a qualitative study of the composites. Clusters where both jets are present and overlap zonally (double jets) are located on the right side of the

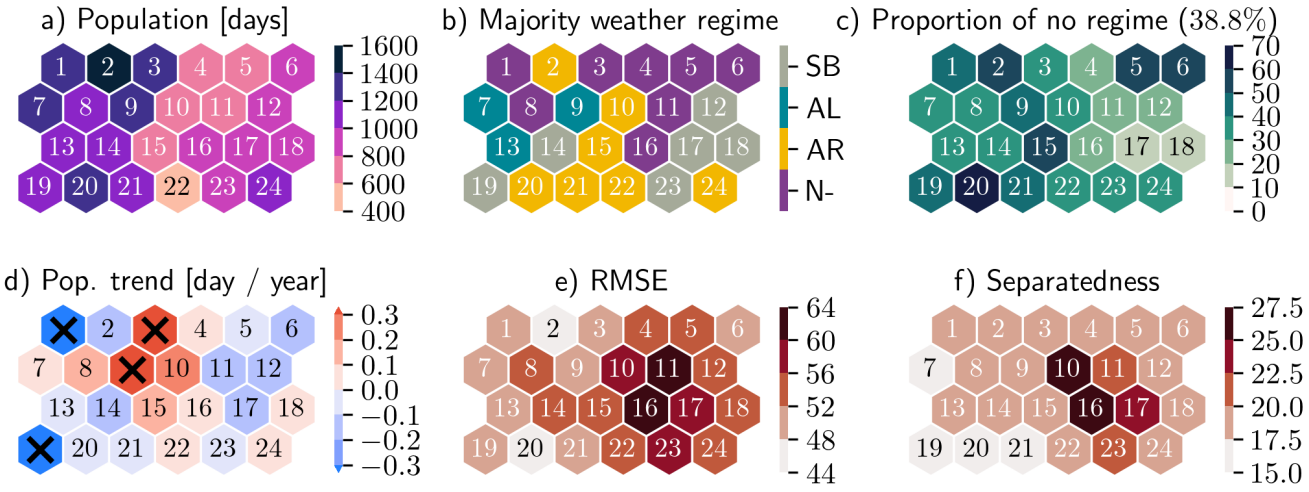

Figure 6. Climatological SOM cluster-wise properties. a) Population, in number of ~~6-hourly timesteps~~ days in JJA 1959 to 2022. b) ~~Daily NAO anomalies averaged over timesteps corresponding~~ Weather regime with maximum relative occurence frequency to ~~a~~ each SOM cluster, excluding "no regime" the shorthands correspond to NAO- (N-), Atlantic Ridge (AR), Atlantic Low (AL) and Scandinavian Blocking (SB). ~~No significance testing is done here.~~ c) Proportion of timesteps withing each SOM cluster not associated with any weather regime, as in Grams et al. (2017), in percents. d) Trends (1959 - 2022) in population in days per JJA. Significant trends at the 95th percentile are marked with ~~a~~ black ~~cross~~crosses. e) Root mean square error of each cluster. f) Separatedness of each cluster, as defined in the main text.

grid and the bottom row. A subsection of this high-overlap region of the grid on the center-right columns, clusters 16, 17, 22 and 23, have the subtropical jet over the Sahara while for most the other clusters with double jets, the ~~centre right region has shorter or even absent and north-shifted STJs, leading to smaller overlaps. Two clusters (7 and 19) on the left edge have very short STJs, as on the right edge. The jets at the lower left and right edges are at lower latitudes~~STJ is further north above the Mediterranean. The EDJ is ~~wavier in the center rows and straighter in the extremal rows. There are a lot of finer scale features in the individual clusters , including some known weather regimes: Scandinavian blocking (clusters~~ especially wavy in clusters 2~~and 22), Atlantic ridge (clusters 16 and~~ , 6, 9, 12, 13, 14, 17~~), and Greenland blocking (clusters 6 and 7). This can be supported by looking at geopotential height anomaly composites in Fig. ?? in the Appendix. Some neighboring clusters whose centers look similar might have differences in intensity or other properties of the jet that are hard to perceive on composite maps, but that will be highlighted when projecting the jet properties onto them in section ??~~, 18 and 24. Clusters 11 and 16 contain more noisy and small scale jet features than the rest of the SOM. In the composites of cluster 2, the region of high wind speed at the eastern edge that could be interpreted as a STJ is too weak and short in the domain to be captured by the jet detection algorithm.

3.2 ~~SOM statistical properties~~

~~Figure ?? shows three~~

Figure 6 shows six SOM cluster-wise properties using a ~~honeycomb~~ hexagonal grid representing the SOM~~clusters~~. The first property (panel a) is the cluster population. There is up to a factor > 3 between the least and the most visited cluster, and the left side of the SOM, featuring shorter and weaker STJs, is a lot more represented than the right side. The least populated ~~clusters, 1 and 7, both feature shorter southward shifted jets~~cluster, 22, corresponds to a south-shifted STJ with a wavy EDJ, while the most populated cluster~~number 8, ~~, 2, features both a ~~short EDJ and a long STJwith little overlap over Europe~~strong, elongated and wavy EDJ doesn't feature a visible STJ.

The ~~daily NAO index, shown on the second~~ clusters are related to the summer Euro-Atlantic weather regimes (figure 6b and c) to simplify their interpretation and compare both approaches. This is done by calculating the weather regime occurence probabilities conditional on each SOM cluster occupancy. The most represented weather regime in each SOM cluster, excluding "no regime", is shown on panel b, ~~projects well on the x-axis of the SOM . This shows that the SOM organizes variance in a sensible way, picking up the signal of the main principal component of the circulation variability in the study region. It is~~ while the proportion of timesteps during which a SOM cluster is occupied but no regime occurs is presented on panel c. Clusters 18, ~~however, not a perfect alignment with the SOM axes, showing that the SOM does more than just discretize the feature space of the first two PCs~~12, 17 and 14 are associated with the Scandinavian Blocking regime, and the corresponding relative occurence frequencies are the highest in all the cluster-regime pairs (not shown). This is probably due to the distinctive footprint bloccking has on the jet, a large poleward shift of the EDJ above Europe. Interestingly, cluster 13, which has a very similar jet structure, is not as strongly linked to this regime but instead to the Atlantic Low regime, along with clusters 7 and 9. The NAO- regime is expectedly associated with SOM clusters with very zonal EDJ, (1, 3, 4, 8 and 11) although the conditional probabilities remain low. The Atlantic Ridge is not strongly associated to any SOM cluster in particular, and the "no regime" appears frequently in most SOM clusters, up to 70% of the time.

In ~~the third panel c, JJA~~ panel d, inter-annual population trends are shown for all clusters. The most negative ~~trends in population(clusters 2, 10, 17) correspond to , respectively, a Scandinavian blocking, a deep Atlantic ridge with weak jets, and a strong wavy EDJ accompanied by a shortand weak STJ with little overlap over eastern Europe. The strongest positive trend, on cluster 24, represents a very similar situation to cluster 17, which showed a negative trend. However, upon closer inspection, it can be observed that the STJ is even weaker and shorter, going below the detection threshold of the jet detection algorithm, and the EDJ is wavier on a shorter wavelength, accompanying geopotential height anomalies in different places over Europe, ultimately resulting vastly different weather situations on the surface. Comparing the trendswith the projected NAO indicates an overall weak trend towards more negative NAO and less positive NAO, in accordance to~~ trend in population, ~~e.g., Harvey et al. (2023).~~ cluster 1, corresponds to a zonal EDJ and a short, north-shifted STJ and is strongly associated to NAO- (panel b). The second most negative trend, cluster 19, features a zonal EDJ and weak, north-shifted and elongated STJ and is not strongly associated to any weather regime. The strongest positive trends, (clusters 3 and 9), correspond to strong EDJ situations, one zonal (3) and one wavy (9), as well as weak and short STJs, without strong association to any weather regime.

~~The appeal of the SOM in the context of characterizing a complex dynamical system like upper-level Euro-Atlantic circulation is the ability to study high-dimensional time series in a much simpler form; as a series of transitions between clusters separated~~

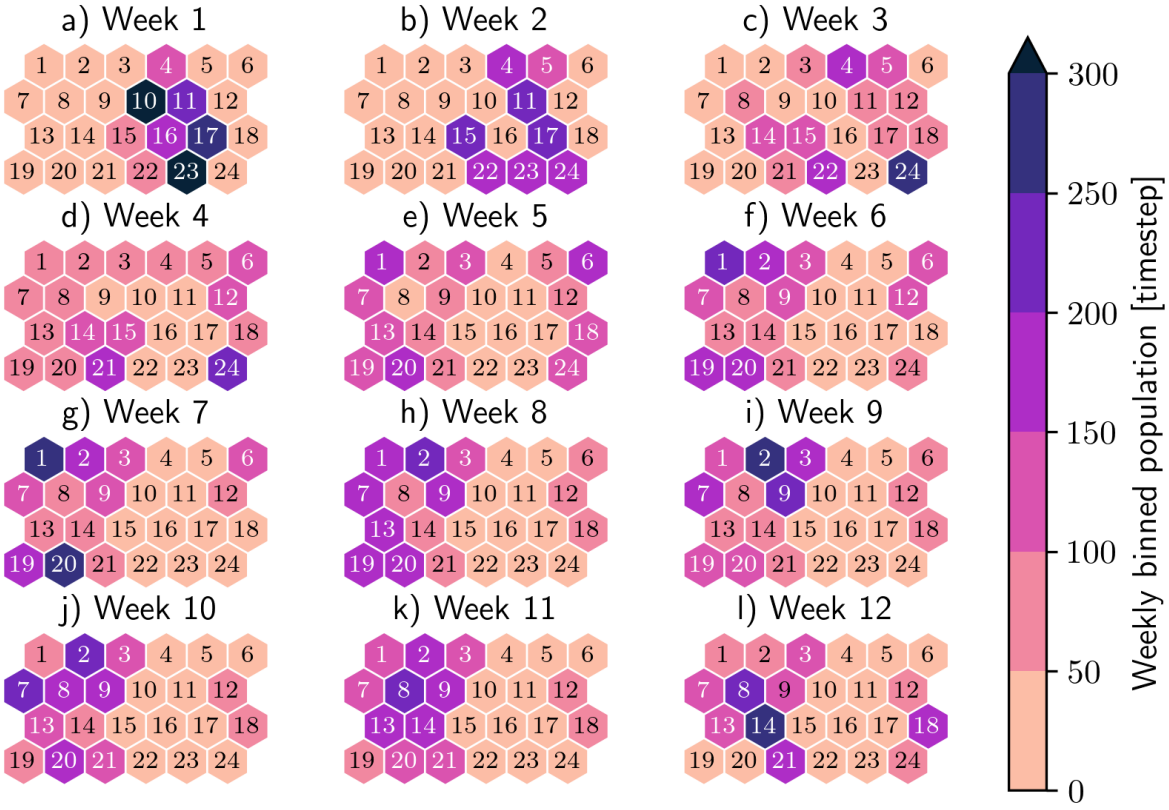

Figure 7. Weekly ~~summer~~ JJA pathway, the weekly-binned cluster population for all weeks of ~~summer~~ JJA and averaged over all ~~summers~~JJAs. Week 1 corresponds to the first week of June and week 12 to the previous to last week of August.

~~by long or short stays. The distance-preserving property of the SOM makes the magnitude of the jumps also meaningful, as opposed to other clustering methods. The link back to upper-level flow is easily made by studying the composites in figure 5~~We also provide two quality metrics for each SOM cluster: the associated RMSE error (figure 6e), where a high value represents a cluster whose weight matrix is a poor representative of many of its members, and the separatedness (figure 6f), where a low value represents a cluster whose weight matrix is very similar to that of its neighbors. We see hotspots in both RMSE and separatedness for clusters 10, 11, 16 and 23. These clusters contain more diverse synoptic situations (high RMSE) than the other clusters, and that are different in their mean to the rest of the clusters, especially those close to them on the grid.

~~Nextwe add a temporal dimension by looking at the typical summer~~ Next, we show the typical JJA pathway through the SOM in figure 7. This figure shows weekly-binned cluster populations for all weeks of JJA and averaged over all ~~summers~~ JJAs 1959 to 2022. It shows that ~~the small isolated~~ a small subset of clusters ~~2,8,13 corresponds to patterns that represent most of early June's circulation , while the rest of the clusters are~~ in the center-right columns of the SOM represents most of the circulation during the first week of June, while clusters on other columns are much more likely to be visited in July and August,

indicating a marked transition of the ~~flow during June~~circulation patterns during June, in the mean over all years. The shift from ~~left to right~~ the center right columns to the center left and edge columns of the SOM grid at the end of June corresponds to a reduction in double jet occurence ~~in JA that will be highlighted in later sections. Cluster 13 corresponds to a negative NAO in early June and cluster 2 to a positive NAO in early June, cluster 8 to an almost neutral NAO state~~and an increase in mean STJ latitude, particularly in July and August.

~~The circulation during these first weeks of June~~is ~~therefore represented by~~ The first week of June, which is climatologically different from the rest of JJA, has its variablity almost entirely constrained to a few clusters~~highlighted earlier. The mean error , 10, 11, 16, 17 and 23 (7). The RMSE~~ on these clusters is higher than for the rest of the SOM (~~not shown) so it is safe to assume that they are the default choice for the early June days but not necessarily good representatives.~~

~~Persistence properties of the SOM clusters. a) Mean residence time. b) 95th percentile of residence times. c) Yearly trend in 95th percentile of residence times in days per decade. Significant trends at the 95th percentile are marked with a black cross. The definition of residence time here is loosened to allow a for a stay to be unbroken as long as the trajectory doesn't leave the radius 1 circle around the starting cluster. The nature of the SOM time series makes it a convenient and powerful platform to study crucial features of dynamical systems such as the persistence. In figure 13, the persistence is characterized using the residence time at a cluster, allowing for departures one cluster away from the origin cluster (see methods~~figure 6e). ~~The residence times are aggregated as climatological JJA averages (panel a) and the 95th percentile (panel b). The JJA averages give an approximation of the state persistence (Tuel and Martius, 2023), i.e., an estimate of how much time to flow typically needs to move from one state into an next state and the 95th percentiles capture more episodic persistence, i.e., the most persistent events of each flow configuration. Decadal trends in the 95th percentile of residence times are shown in panel c.~~

~~Both aggregations (mean and 95th percentile) highlight similar hotspots of high persistence on the top-left and bottom-right corners of the SOM with the exception of cluster 20. However, the high residence times for the clusters in the upper left corner (2~~clusters earlier identified as early June clusters are almost never populated again past the first of July. The clusters on the upper left corner (1, ~~8,13) cannot be interpreted under the same light as the high residence times in clusters 17 and 18. The high residence times in clusters 2,8 and 13 arises from the seasonal pattern, i.e., the circulation resembles theses clusters in early June . The high residence times in clusters 17 and 18 is true state persistence. The most persistent cluster is also the most frequently visited cluster. The least persistent clusters are clusters with a wavy single EDJ, or a short STJ. The clusters with the highest episodic persistence outside the first weeks of June (clusters 17,18, 20 and 23) are quite diverse and fall into neutral (clusters 20, 17, 23) and negative (cluster 18) phases of the NAO, they feature double jets (cluster 20), a straight jet (cluster 18) and wavy jets (clusters 17 and 20). The trends in residence time follow the trends in population from figure **??**. The low number of significant trends and their overall low values suggest that they are probably random.~~ 2, 3, 7, 8 and 9) are the most populated in late July and early August

~~SOM dilution at different backward lags, as defined in methods. A lighter shading on a cluster means that a shorter pathways lead to it.~~

~~As residence time can be seen as a discrete-space equivalent to the dynamical system's persistence factor θ^{-1}, a loose equivalent to the local dimension d and a proxy for predictability is found with the backwards dilution. Note that it is not a~~

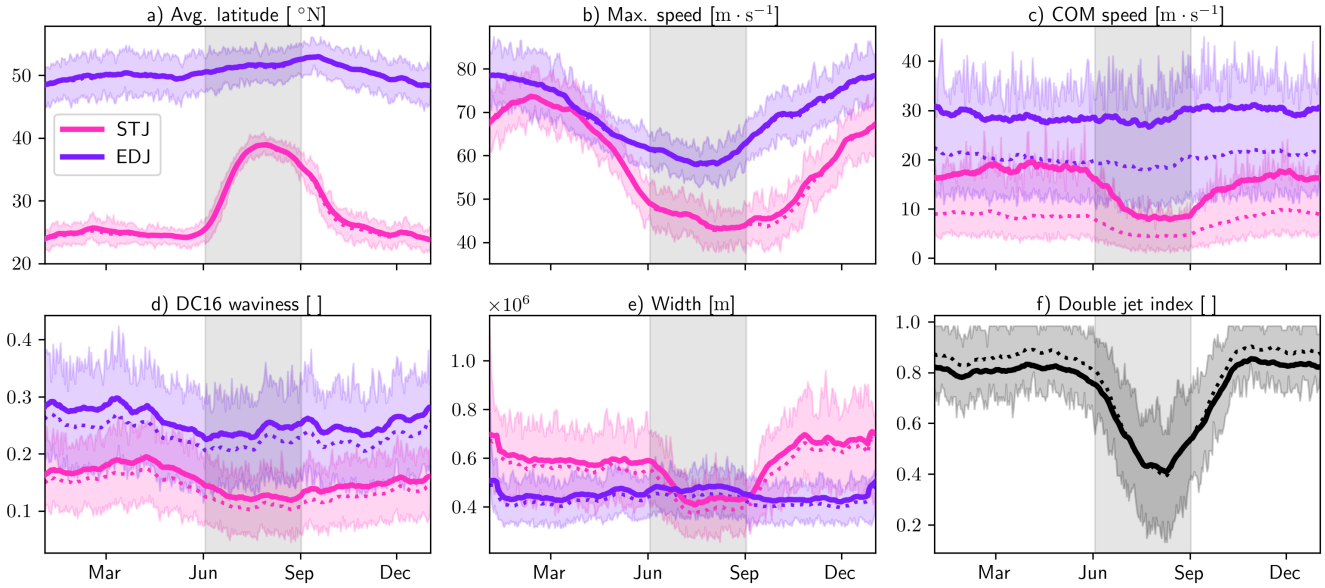

Figure 8. Euro-Atlantic jet properties ~~annual signal,~~ seasonal variability. The results are split by jet category and always colored in the same way: pink for the STJ and purple for the EDJ. The double jet index is colored in shades of gray. A 15-day-window averaging is applied to the day-of-year mean (thick line) as well as the day-of-year median (thin dotted line) but not to the inter-quartile range (shading). The marker label for each month corresponds to the first day of this month. The grey rectangle in the middle of each panel represents JJA.

~~perfect proxy, as it does not account for the likelihood of transitions. Long jumps, say from cluster 1 to 15, might be very likely in the transition probability matrix, and therefore more predictable, but they would still weigh towards a high backwards dilution of cluster 15. Figure ?? shows that, at a timescale of seven days, shorter pathways lead to the high-overlap double jet states on the top-left than to the lower-overlap or even single jet states. Clusters with the highest dilutions (6 and 10) resemble Greenland blocking, which coincides with the low forecast predictability of this regime (Osman et al., 2023). On the other hand, JA clusters with the lowest backwards dilution resemble the Scandinavian Block and Atlantic Ridge weather regimes. Those results are at odds with the findings of Hochman et al. (2021), who identify a low local dimension anomaly d for Greenland Blocking and a higher d for Scandinavian Block and Atlantic Ridge. This discrepancy either comes from a bad correspondence between backwards dilution and instantaneous local dimension, or the fact we only use JJA data. Some JA clusters with lower dilution also have high persistence (e.g., cluster 20), but not always, for example, clusters 17 and 18 being persistent but unpredictable. This means that while the number of SOM space trajectories leading to these clusters that have length 0 is higher than for other clusters, the rest of them have, on average, high lengths.~~

3.2 Jet ~~feature~~ stream properties

From Using the detected and categorized jets, it is now possible to study the jet feature properties . They are numerous we study the properties of each jet category separately. We have defined numerous jet properties and many of them are correlated with one another, so only a selection of six are shown in the main text, while results for a larger selection of variables are presented are presented in Appendix B.

The six properties chosen have all seen keen interest in past literatureunder various formsthe literature. The average latitude can be compared to the Jet Latitude Index JLI (Woollings et al., 2010) while the max. speed can be compared to the Jet Speed Index or JSI or to the 99th percentile of wind speed (Shaw and Miyawaki, 2024). The speed of the(inverse of the) jet's COM speed can be viewed as a proxy for persistence, the R16 waviness(Röthlisberger et al., 2016b) is one of the most natural way to characterize this property . The waviness, as defined by Di Capua and Coumou (2016), and hereafter named DC16 waviness, is a simple metric to quantify the departure from zonality of the detected jet objects, the jets. The width of the jet is emerging as another feature of interest in recent literature (Peings et al., 2018) and is here computed using natural coordinates. Finally, we determine, at each longitude, if both jets are present and average this overlap boolean quantity over the European sector ($\lambda > 10$ °W). The mean latitude, max. speed and width 's distributions have low skew, while the COM speed, waviness and double jet index's distributions are very skewed with tall peaks at low values and long tails.

The yearly cycle seasonal variability of this selection of jet properties is presented in figure 8. All the results are split by jet category and always colored in the same way: pink for the STJ and purple for the EDJ. The double jet index is colored in black. Several interesting features can be observed in this figure. First, the month of June is once more highlighted as a transition month that is different from the rest of summerJJA. More precisely, the speed and width of both jets and the waviness of the STJ reduce in the months leading up to June , with a stronger signal for the STJ(figure 8b and d). Then, during June, both jets move poleward, with again a a much more pronounced shift for the STJ (figure 8a).

The yearly cycle seasonal variability in latitude and speed of the EDJ are very comparable to the Jet Latitude Index and Jet Speed Index yearly cycles seasonal variabilities (Woollings et al., 2014) and the storm track yearly cycles seasonal variabilities (Hoskins and Hodges, 2019) for the equivalent EDJ properties (respectively average latitude and max. speed). The amplitude and width of the summer JJA peak in STJ latitude can be compared with Maher et al. (2020). Seasonally, the STJ follows the expansion and weakening of the Hadley cell in the northern hemisphere summer (Dima and Wallace, 2003; Davis and Rosenlof, 2012), although the relationship between STJ latitude and Hadley cell edge is weakening with global warming (Maher et al., 2020).

The speed of the COM and the R16 DC16 waviness do not show strong seasonal cycles in contrast variabilities in contrast (figure 8c and d), with signals staying well below the interannual variability, although a dip in STJCOM speed and in EDJ waviness are still noticeable in late summer . Both jets show a clear summer decrease in their widths. The EDJ width is smooth and quasi sinusoidal, while the STJ width jumps from a constant regime to the other in June and October. The with the exception of the STJ's waviness which shows a peak in spring. The jets are much closer together in summer JJA than the rest of the year, but overlap less often, mainly due to the subtropical jet occuring less often in summer. This is likely to affect Rossby wave breaking frequency and intensity. JJA (see 4).

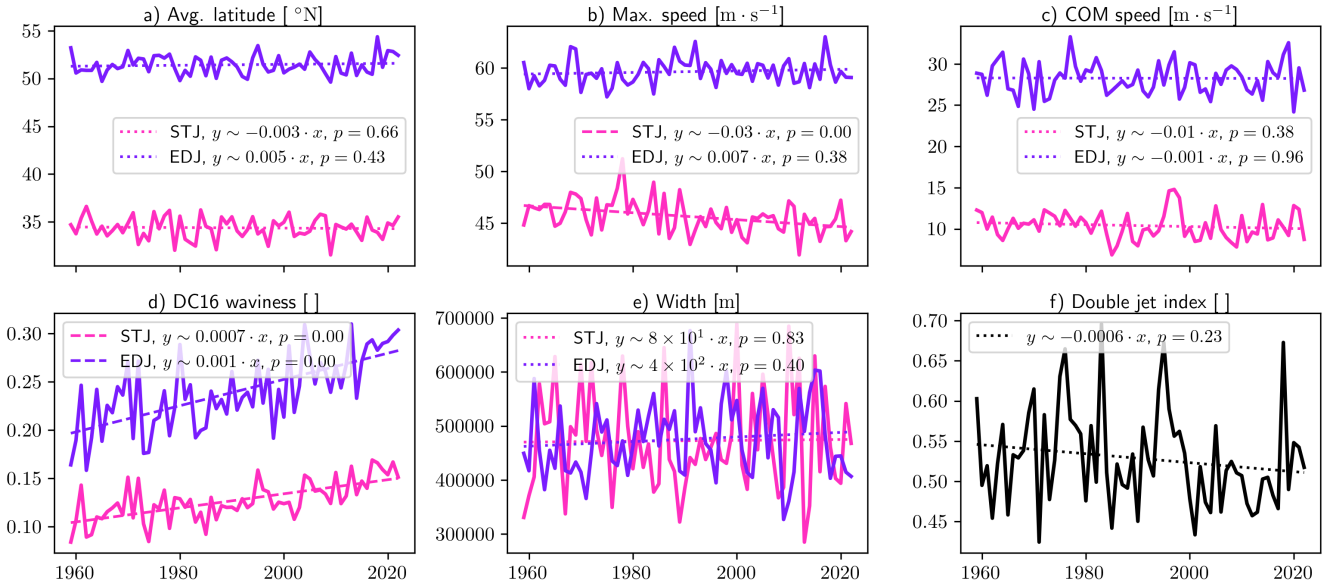

Figure 9. Euro-Atlantic jet properties ~~summer~~ JJA means and inter-annual trends, split by jet category. Linear trends represented by dashed lines are significant at the 95th percentile, while the dotted lines are not.

~~Euro-Atlantic jet properties all-year trends, split by jet category. Linear trends represented by dashed lines are significant at the 95th percentile, while the dotted lines are not.~~

An important questions is how these properties have evolved under the past climate change. Figure 9 shows the inter-annual JJA trends for the selected six properties~~, while figure ?? shows the all-year trends for the same six properties~~. Statistical significance is tested using block bootstrapping, with 10000 bootstrapped time series created with a block size of four years.

Trends in ~~summer~~ JJA are yet to emerge out of the ~~inter-summer~~ inter-annual variability, as only ~~two~~ three of the eleven trends shown in figure 9 are significant, ~~negative trends in the width and max.~~ a negative trend in the max. wind speed of the STJ ~~. This STJ~~ and a positive trend in the waviness of both jets with the DC16 definition. The STJ max. wind speed trend is consistent with the findings of D'Andrea et al. (2024), who report a significant decrease in zonal wind between -0.1 and -0.5 m/s per decade ~~in the area highlighted as the preferred positions~~ an the area corresponding to the location of the STJ in ~~summer in figure 4. The trend in STJ width has, to our knowledge, not been explored in the literature. The poleward shift of the EDJ projected in, e.g., Held (1993), is not present in these results in summer, nor is the equatorward trend of the STJ reported by Totz et al. (2018). The absence of a trend in STJ latitude, seemingly at odds withthe measured tropical expansion (e.g. Davis and Rosenlof, 2012), is consistent with findings in the recent literature (Davis and Birner, 2017; Maher et al., 2020) . The absence of a trend in the persistence proxy for jet objects, the speed in their COM, is in agreement with the small trends in SOM cluster residence times presented earlier. This agreement is to be contrasted with the poor correspondence between state persistence (SOM cluster residence times) and flow persistence (low COM speed)highlighted in section ??.~~

Trends in the annual mean are clearer in contrast, thanks to strong signals in the cold season in particular. Some trends, like for the double jet index, even change signs between summer and all-year. The poleward shift of the EDJ is slow and not significant. Its sign is in accord with Held (1993) and more recent work also studying future simulations (Barnes and Polvani, 2013; Lachmy . The increase in jet maximum speed is reminiscent of the "fast-get-faster" observation in future simulations by Shaw and Miyawaki (2024) and can also be related to longer-term JJA (see figure 5). The trends in mean jet speed (Woollings et al., 2018a; Harvey et al., 2023) waviness, while large in this figure, are dependent on the definition, as we showcase in Appendix B. An increase in waviness in this region is consistent with, e.g. Francis and Vavrus (2015) and Cattiaux et al. (2016). It is also consistent with a positive trend in occurence frequencies for SOM clusters featuring wavy or tilted (3, 9) and negative trends in clusters presenting more zonal jets (1 and 19). It is worth mentioning that, with our definition, there is only a non-significant negative trend in double jet index in this domain. The slow but significant increase in EDJ waviness over time is not robust to a change of period (see table **??**), in accord to findings by Blackport and Screen (2020a). The squeezing of the jet, along with the increase in speed, coincides well with the findings in Peings et al. (2018). The increase in waviness is consistent with Francis and Vavrus (2015) , Di Capua and Coumou (2016) and Cattiaux et al. (2016) .

More trends of these six jet properties can be viewed in table **??**, for the full ERA5 period as well as for a restricted period corresponding to available satellite imaging, 1979-2022, where the reanalysis data is more robust but even more limited in time and in this sense statistically weaker. An extended version of this table with more variables, table **??**, can be found in the Appendix. Expectedly, most trends are similar in the two periods, with typically small changes in the value or significance of the trend. It is worth mentioning a few trends that change signs between the two periods, for example the MAM STJ max. speed. Most trends discussed in the previous paragraphs are however valid in both periods, conserving signs and intensities but sometimes losing or gaining significance when computed on

Trends of these six jet properties can be viewed at a finer temporal scale, for each day of the year on figure 10. The significance is once more established using block bootstrapping with the same settings as for figure 9, and it is assessed prior to the 60-day rolling-window smoothing.

The EDJ exhibits a poleward shift accross most seasons, consistent with the arguments of Held (1993) (figure 10a). The STJ shows an equatorward trend in spring and a poleward trend in autumn (figure 10a). The EDJ maximum wind speed increases consistently accross the whole year, with the strongest of intensification in February, March, May and June (figure 10b). This result can be linked to results in past data (Woollings et al., 2018a; Harvey et al., 2023), and in future simulations Shaw and Miyawaki (2024). The STJ has opposite trends in its max. speed between JJA, where the trend is negative, and September to December where the trend is positive (figure 10b). No strong trends appear in our results for the COM speed, except a negative trend in COM speed in July and August for the EDJ and in Sepember and October for the STJ (figure 10c). DC16 waviness increases significantly, for both jets and consistently over the whole year, with a stronger increase between January and June (figure 10d), which is mostly consistent with , e.g. Cattiaux et al. (2016) and Di Capua and Coumou (2016), albeit in different regions. The width does not show strong trends except a negative trend in April and May for the STJ (figure 10e). Finally, the shorter period. Finally, a finer evolution of yearly trends accross seasons can be seen on Appendix figure B2 and shows interesting seasonal shifts in yearly trends, typically around the month of june again. This suggests that the usual

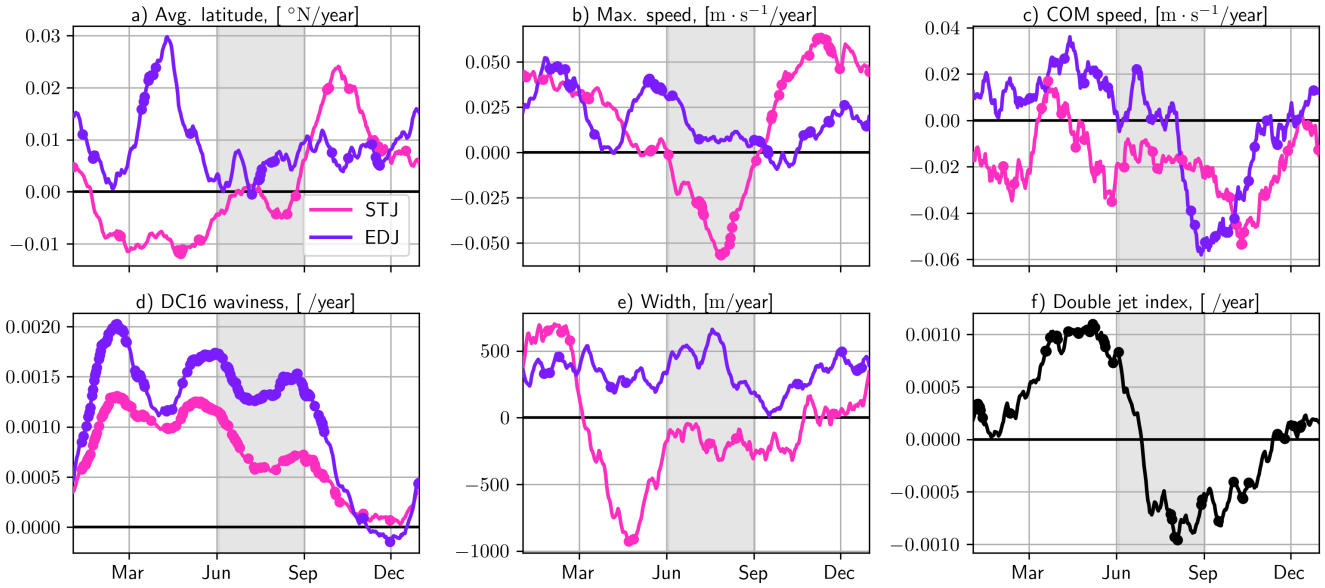

Figure 10. Euro-Atlantic jet properties inter-annual trends, computed independently for each day of the year, and the result smoothed by a 60-day rolling window. Trends significant at the 95th percentile are marked with a thick dot. Significance is assessed prior to smoothing.

~~seasonal separation that we used on figure 9 and table **??** might not show the full complexity of the seasonally varying trends. 1959- 1979- 1959- 1979- 1959- 1979- 1959- 1979- 1959- 1979- Avg. latitude STJ −1.5 1.5 −7.8 −12 −14 −8.2 7.1 **25** −**6.7** 0.32 [10^{-3} °N/year] EDJ 8.8 5.9 11 11 −2.6 6.5 0.8 6.4 4.6 7.4 Max. speed STJ **3.5** 2.4 1.9 −2.9 −**3.3** −3.2 **3.4** **5.6** **2.4** 0.98 [10^{-2}m · s^{-1}/year] EDJ **2.9** 3.8 **2.3** **6.6** 1.2 −0.12 **2.8** 1.4 **2.3** **2.9** R16 waviness STJ 2.5 1.5 −3.4 −**14** 9.8 −0.42 12 15 4.2 −0.33 [10^{-4} °N/ °E/year] EDJ 59 85 23 −95 7.3 −79 **78** 36 **42** −14 Width STJ −**1.8** −1.6 −0.46 −**2.1** −**1.1** −1 −**0.9** −0.33 −**0.84** −**1.2** [10^{3}m/year] EDJ −**0.62** −**1.5** −0.26 −0.43 −0.25 −0.11 −0.36 −0.52 −**0.37** −**0.63** Speed of COM STJ −14 7.8 20 −4.9 −24 −17 −14 32 −4.3 6.9 [10^{-3}m · s^{-1}/year] EDJ −3.5 7.1 5.9 **23** −11 2.1 −**14** −18 −5.7 4 Double jet index [10^{-4} /year] **5.4** 8.2 **13** **21** −3.1 −1.2 −0.74 3.6 **3.6** **7.9** Summary of jet property feature trends for all seasons and the periods 1959-2022 and 1979-2022. Trends are expressed per year and significant trends at the 95th percentile are written in bold.~~ double jet index increases significantly in March, April and May and decreases significantly in July and August (figure 10f), although the trends in JJA averages were not significant (figure 9).

3.3 Jet properties on the SOM

In this section, we make use of the detected jets and their properties to assess the capabilities of the SOM to capture jet stream variability as opposed to random noise. First, we composite jet core detection probability, separated by jet category, and overlay on top the jet cores found in the SOM wind speed composites, i.e. figure 5. The results, visible on figure 11, show a clear agreement on the position of the detected jet cores as well as on their categorization.

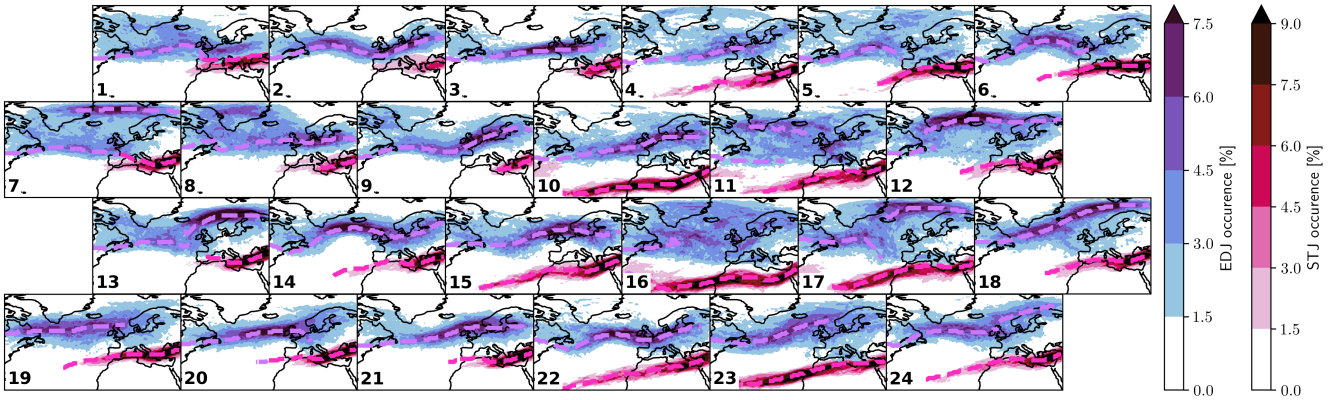

Figure 11. Jet core detection probability composites (blue shading for EDJ, pink shading for STJ), and jet cores found on wind speed composites, figure 5, as colored lines (purple for EDJ, pink for STJ).

As a way to compare and validate the results of both methods, a selection of jet properties are projected onto the SOM clusters, shown in figure 12. ~~The observations made on the latitudinal positions of the jets,~~

The latitude of the EDJ is, as on the composites, higher on the extremal columns than in the central columns of the SOM (panel a), and the clusters with highest mean EDJ latitude also correspond to clusters with high relative occurence of the Scandinavian Blocking weather regime (see figure 6b). The maximum speed of the EDJ is highest on clusters 10, 14 and 23. These three clusters have the highest population during the first (10 and 23) or the last (14) week of JJA (see figure 7), when the EDJ has the highest max. speed in JJA (see figure 8). Similarly, the EDJ max. speed is lowest in clusters populated in the middle of JJA (clusters 1, 7, 12, 19, 20). The EDJ waviness is highest on most cluters associated to the Scandinavian blocking or Atlantic Low regimes, and lowest for clusters associated to the NAO- or Atlantic Ridge regimes, with the notable exception of cluster 8, weakly associated with NAO- but very wavy (see figure 6b, relative occurence not shown).

The double jet index, as well as the ~~jet overlaps,~~ max. speed, mean latitude and width of the subtropical jet all follow the very clear seasonal signals presented in the previous section (figure 8) when matched with the weekly cluster populations (figure 7). The observations are also very consistent with what can be seen on the jet core probability composites (figure 11).

The observations made, qualitatively, on the wind speed composites (figure 5), can all be matched with the jets' mean ~~average latitudes and the mean double jet index~~properties on the clusters (figure 12). This result is not entirely trivial. It means that, for most clusters, the jets found in the cluster mean wind speed composites have properties corresponding to the mean of the properties of the jets found in each individual timestep belonging to that cluster. In other words, the wind composites and the jets found therein are representative of the wind speed snapshots, as well as their jets, belonging to each cluster and not merely artifacts of averaging noisy fields. These observations are quantified in Appendix C.

~~Results from the projection of COM speed seem to indicate that persistence characterized as a slower movement of the jets' COM can hardly be reconciled with the persistence characterized as longer stays on a given SOM cluster, as slow COM speed~~

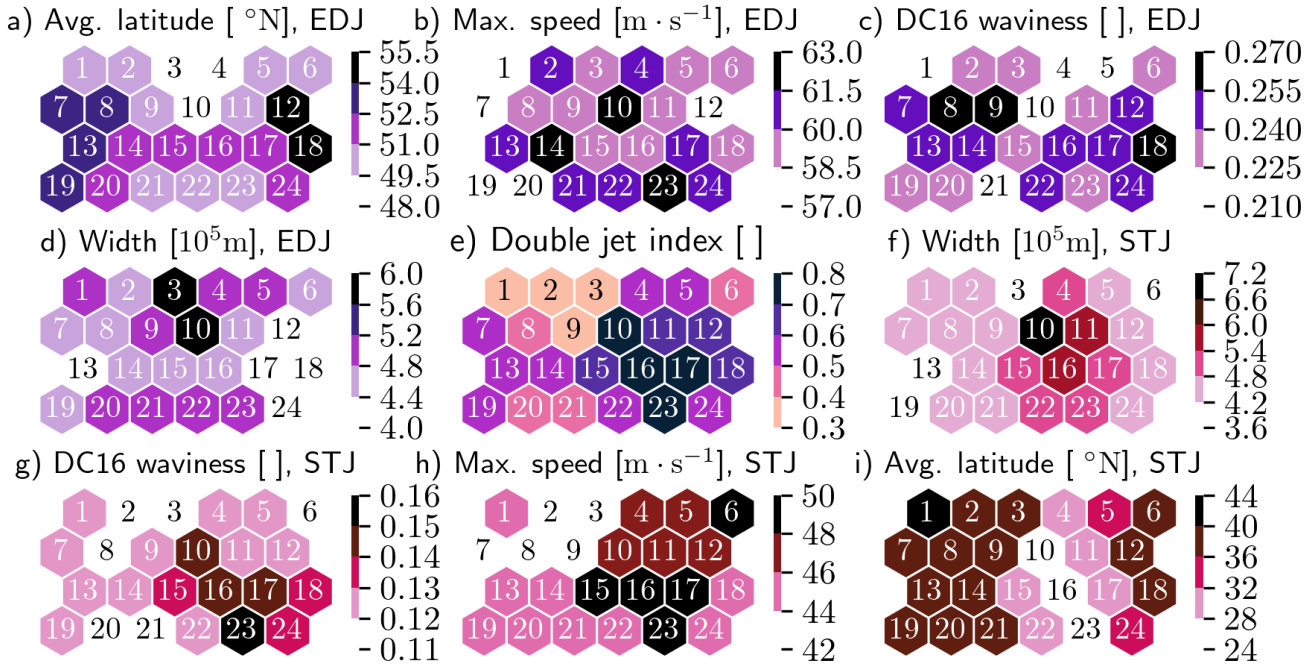

Figure 12. Jet properties, separated by jet category when applicable, projected on the SOM clusters. Shades of purple corresponds to EDJ properties and shades of pink to STJ.

3.4 Jet persistence

We characterize persistence using three metrics extracted from the residence times on each SOM cluster and two metrics for each jet category, the jet lifetime and the speed of the center of mass. To compare all of these metrics, we aggregate their results for each SOM cluster and plot the results in a hexagonal plot as in section 3.3.

Our definition of residence times allow for departures one cluster away from the origin cluster (see section 2.2.3). We first count the number of stays that last more than 4 days on each SOM cluster (figure 13a). The lengths of stays of any length are aggregated as JJA averages (panel b) and 95th percentiles (panel c). The summer averages give an approximation of the state persistence (Tuel and Martius, 2023), i.e., an estimate of how much time the large scale-scale circulation pattern typically needs to move from one state into the next, while the number of long stays and the 95th percentile of residence times capture more episodic persistence, i.e., the most persistent events of each flow configuration.

Clusters 1, 2, 3 and 20 are characterized by a large number of long stays, and a high state and episodic persistence. These clusters all represent a roughly similar synoptic situation of a zonal EDJ extending over the British Isles and with low positive tilt, but with minute differences in apparent EDJ waviness and length of the STJ. These are very well-defined clusters (low RMSE) but with the lowest separatedness in the SOM, which confirms our observations on their composites. In the rest of the

SOM, the state and episodic persistence seem to be correlated, and the previously highlighted region of clusters representing the first week of June (10, 11, 16, 17 and 23) does not stand out as more or less persistent than the clusters representing the rest of JJA.

Results from the projection of jet-wise persistence metrics onto the SOM show mixed agreement with the SOM persistence metrics, at least in this presentation of temporal aggregates, as well as mixed agreement among each other. High COM speeds of either jet~~are as likely to~~ , indicator of low instantaneous persistence, can be associated with ~~long residence times (see again figure 13) as with short ones. This discrepancy is a great motivator for future work on the different facets of this important feature of circulation.~~ either low or high state persistence, and with either low or high jet lifetime, for jets of the same nature or the other. It is worth reminding that, while all of these numbers characterize persistence in some sense, they are very different in nature. Jet lifetime and SOM average residence time are both nonlocal, which means they can only be determined when a jet has weakened below the jet integral threshold or left the domain, and when a stay on a SOM cluster has ended. Additionally, the two jet related metrics only assess the persistence of one jet at a time, which can be very different. This can make these metrics unfit to qualify a timestep or a period concisely.

4 Discussion and summary

We use two complementary methods~~(SOM and jet features)~~ , self-organizing-maps (SOM) and jet core detection, to characterize the upper-level tropospheric jets, and apply them to the Euro-Atlantic sector in the less studied northern hemisphere summer season, along with some year-round results. The SOM method specializes in finding dynamical properties of the overall flow, including persistence~~and predictability~~, while the jet ~~features~~ core detection method finds properties of individual jet ~~feature~~ cores at every timesteps, ~~of which we present trends and seasonal signals~~and present for each the ERA5 inter-annual trend and intra-seasonal variability. These methods have overlaps, for example the SOM shows a clear ~~seasonal signal~~ intra-seasonal variation in cluster population, and some of the jet ~~feature~~ properties are proxies for persistence. These overlaps allow us to verify the results between methods, increasing our confidence in our results.

The ~~self-organizing map (SOM), a data-driven~~ SOM, a clustering method with distance-preserving properties, allows us to study the circulation time series as a sequence of stays on a cluster and jumps between clusters, where the magnitude of the jumps is meaningful. ~~This can be directly applied to the evaluation of persistence and predictability. The SOM was able to highlight circulation patterns exhibiting high persistence times, a natural characterization of~~ A group of clusters with low population, high mean cluster error, high cluster separatedness, and a south-shifted STJ compared to the other clusters, is shown to be comprised almost entirely of timesteps in the first one or two weeks of June every year. This time of the year is therefore identified as having a very different mean synoptic situation to the rest of JJA, but its relatively low weight in the data compels the training algorithm to only assign a few clusters to it, too few to correctly capture the variability of this period.

The SOM is related to weather regimes using relative occurence frequencies. With strict conditions for regime occurence, a high proportion of JJA days is not assigned to any regime, and only a few SOM clusters can be strongly associated to weather

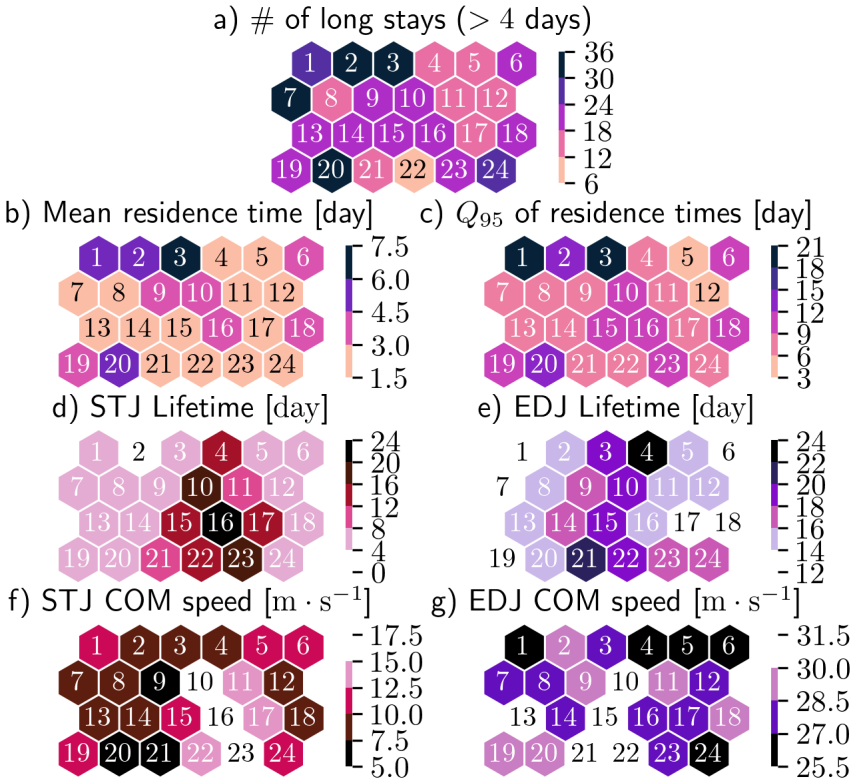

Figure 13. Persistence properties of the SOM clusters. a) Number of long stays on each SOM cluster. b) Mean residence time on each SOM cluster. c) 95th percentile of residence times on each SOM cluster. The definition of residence time here is loosened to allow a for a stay to be unbroken as long as the jumps are to a cluster similar enough to the starting cluster (below the 10th percentile of pairwise distances between cluster weight matrices). d-g) Jet persistence properties, separated by jet category when applicable, projected on the SOM~~clusters~~. Shades of purple corresponds to EDJ properties and shades of pink to STJ.

regimes, typically to the Blocking regime which is accompanied by a poleward shift of the EDJ above Europe, easily captured by our wind-based clustering approach.

Long stays on a SOM node is a natural way to evaluate state persistence. The most persistent ~~patterns both correspond to a strong zonal EDJ extending far inland over central Europe and a short STJ over southern Europe. A proxy for predictability on the SOM grid,~~ clusters correspond to long EDJs that extend over the British Isles, and north-shifted, short and weak STJs over the ~~backwards dilution, found patterns that are typically reached from neighboring clusters~~ Mediterranean. Aside from those rough similiarities, they present differences in EDJ waviness and maximum speed according to the mean jet properties projected on the SOM~~rather than far ones. Clusters with low backwards dilution resemble the Scandinavian Block and Atlantic Ridge weather regimes. The SOM was also able to identify the seasonal shift from early to late June, that is confirmed using the jet feature method. Trends in clusters exhibiting certain properties (high overlap of the jets over Europe, blocking) and~~

weekly means of cluster population were also extracted to be compared against the results of the jet feature method showing high consistency. The SOM highlighted known the large scale trend towards more negative NAO in summer, as well as trends in many smaller scale features. These clusters, which have high occurence probability and persistence, typically do not project well on any weather regime. This is a strong incentive to consider using more clusters than four, irrespective of the clustering method employed, when it is compatible with the research question. In this study, the larger number of clusters has allowed us to describe the majority of JJA timesteps as cluster visits with low projection error, and has all but guaranteed that all the persistent episodes can be extracted as long stays on SOM nodes, with our definition.

A variation of the jet core detection algorithm presented by Spensberger et al. (2017) is used to identify instantaneous jet features and extract per-feature jet properties . The jet features are tracked to obtain metrics offering another view of persistence, and jets and extract properties for each of them separately. The jets are classified into the two canonical jet categories (subtropical and eddy-driven jet, resp. STJ and EDJ), and tracked over time to obtain metrics that offer another view of persistence. Once more, past trends and seasonal signals are extracted. In summer

In JJA, the only significant trends are a decrease of the width an increase of the DC16 waviness of both jets and a slowdown of the STJ. This latter trend is consistent with the literature, while the former is, to our knowledge, novel. Over the whole year, we find a significant poleward shift and an increase in waviness of the EDJ, a decrease in width and increase of the maximum speed of both jets, and a decrease of the average latitude of the STJ. The persistence metrics developed around the jet feature method seem to show another facet of persistence to the one expressed by the SOM cluster residence time, and the results of both methods often disagree. However, both methods agree that no aspect of persistence is either increasing or decreasing in timeThe poleward shift of the EDJ projected in, e.g., Held (1993), is not significant in our analyses in JJA, nor is the equatorward trend of the STJ reported by Totz et al. (2018). The absence of a trend in STJ latitude, seemingly at odds with the measured tropical expansion (e.g., Davis and Rosenlof, 2012), is consistent with findings in the recent literature (Davis and Birner, 2017; Maher et al., 2020).

Year-to-year trends, computed independently for every calendar day, vary a lot over the year at subseasonal timescales. The trends in 3-monthly averages that are often presented in literature can therefore sometimes be misleading, as they can average out strong trends of opposite signs. As an example, the double jet index has a strong positive trend before and up to June, and a strong negative trend in July, August and September, so its trend in JJA average is weakly positive. Still, it is useful to continue discussing these trends in seasonal averages, to create points of comparison with the past literature and because they allow us to illustrate the different amounts of interannual variability between jet properties.

Comparing results from the two methods, SOM and properties of the detected jet cores, helps to validate them. The subjective jet SOM is shown to capture jets and not random noise, because the jet cores detected on the composited wind fields match very well with the probabilities of jet core detection, composited for every cluster. The expert-defined jet properties do succeed in characterising features which dominate the leading patterns in the more objective statistical SOM approach. Computing the properties the jet features of every timestep properties of the jets at every time step before averaging them based on cluster membership gives very close qualitatively similar results to computing jet properties on the jet features cores extracted from each cluster wind speed composite. This indicates that both methods are coherent with one another. , but the match is not perfect.

Furthermore, the strong ~~seasonal~~ regime shift happening in June, characterized most clearly by a weakening and poleward shift of the STJ, is distinctly picked up by both methods. Trends in waviness can be matched to positive trends clusters with wavy or tilted jets. As a more subtle point, clusters that represent early June and have the highest mean double jet index within this subset get more frequent, albeit weakly, than the rest of this early June subset, while the opposite is true for the July-August subset of SOM clusters, which matches well with the opposite sign trends in double jet index between early and late northern hemisphere summer. This indicates that both methods are mostly coherent with one another.

The ~~jet detection~~ persistence metrics developed around the jet detection method show another facet of persistence to the one expressed by the SOM cluster residence time, and the results of both methods often disagree. This is partly explained by their many differences in nature. Only the jets' COM speeds can be assessed locally in time, and the jet related metrics only refer to persistence of a single object at a time, different from the state or episodic persistence quantified by SOM residence times.

The jet detection algorithm is directly applicable to global data, as are the jet properties computation and the jet tracking. A global jet categorization would, however, have to use an adapted set of jet properties to distinguish the EDJ from the STJ, as longitude and latitude are only good discriminants in the Atlantic basin. A different set of jet properties might have to be used for each season or even each month, as the seasonal signals suggest. The SOM, like all clustering metrics, is not well suited for a global application and works best when restricted to a single basin. The steep increase in dimensionality and variability that accompanies an expansion to a larger region, combined with the same proportionally small number of timesteps, creates a much more ill-defined clustering problem. Since both methods are relatively cheap computationally, they can be applied to large ensembles and higher-resolution model data to evaluate future trends and shifts in seasonal signal or persistence and predictability properties.

In future work, we will use these diagnostic tools to study the circulation before and during extreme weather events in Europe. Potential applications currently explored include assessing atmospheric persistence and predictability properties in the days leading up heatwaves, finding SOM clusters most likely to see the onset of a damaging hail storm, and discovering which jet properties can be used as good ~~statistical~~ predictors for extreme surface winds in a statistical model.

The previous paragraph pertains to the jet stream as a potential driver of weather predictability, even if the causality can go in both directions. Another use for the methods is the investigation of the drivers of jet stream variability, for example, large-scale teleconnections like ENSO or local mechanisms like diabatic warming, as has been studied recently by Auestad et al. (2024). Another avenue is the exploration of the jets' tight relationship to Rossby waves, for example by assessing the ~~waveguidability~~ ability of the detected jets ~~(Martius et al., 2010; Wirth, 2020; Bukenberger et al., 2023; White, 2024)~~to carry and guide Rossby waves (Martius et al., 2010; Wirth, 2020; Wirth and Polster, 2021; Bukenberger et al., 2023; White, 2024). Similarly, it is now easier to examine their relationship to Rossby wave breaking, for instance as triggers of large jumps in SOM clusters (Michel and Rivière, 2011), or as drivers for abrupt changes in jet strength, latitude, or center of mass speed (Martius and Rivière, 2016). Adapting the jet width method to instead find wave breaking events around the jet core is showing promising early results.

Code and data availability. The ERA5 reanalysis data are publicly available at https://cds.climate.copernicus.eu. The SOM training and visualization code (hexagonal plots) was adapted from https://github.com/fcomitani/simpsom, and the rest of the code can be found at https://github.com/hbanderier/jet_stream.

Appendix A: ~~More SOM composites~~Further exploration in jet categorization

~~Once the SOM is trained, composites of any other field can be computed by averaging this field over timesteps belonging to each cluster. On Figure ??, we perform this on geopoential height anomalies at 500 hPa to provide more familiar patterns to read and , for example. compare to~~ On figure A1, we explore the effects of changing the categorization method on the seasonal variabilities of the categorized jet properties. First, on the first three rows of the figure, we vary the cutoff between STJ and EDJ. The effects on the mean position (in latitude and pressure level) is barely distinguishable, but the effects on the number of jets of each category per timestep can be markedly altered by this choice, especially for the STJ when changing the cutoff from 0.1 to 0.5.

Then, we allow jets whose categorization score is between 0.1 and 0.9 to be assigned to the hybrid category. The aggregated properties for the three jets can be seen on the fourth row of figure A1. As many jets belong to the hybrid category as to the ~~usual weather regimes. To remind the reader of the underlying wind fields used to train the SOM, the jet features found in each cluster are overlaid on the composites using the same color code as~~ STJ in winter, while in JJA there are more hybrid jets than STJ, according to this cutoff. However, this hybrid jet has an almost identical seasonal cycle to that of the STJ, in its spatial distribution but also in its other properties (not shown). We therefore decided against introducing this third category in the paper, since it seems to behave like a STJ. This is also why we choose a cutoff of 0.9 in the main text. ~~The position of the jets around positive and negative geopotential height anomalies are an indication that the SOM cluster composites seem physically sound and coherent with one another. Composites of 500 hPa geopotential height anomaly for all days corresponding to a cluster, and result of the jet core detection algorithm overlayed as colored lines; pink for STJ and purple for EDJ. The SOM cluster number is indicated by a number in the bottom left corner.~~ This way the STJ corresponds to well defined STJs as well as hybrid jets which we identify as worse-defined STJs.

We would interpret these findings as follows. In JJA, the subtropical jet is shifted north with the Hadley cell and interacts with extratropical eddies more, making it lose more momentum (Martius, 2014) and potentially making it more baroclinic. This makes the distinction more fuzzy, so there are more jets that don't fall cleanly on either Gaussian, i.e. more jets with a score very different from either 0 or 1. These jets still seem to behave more like STJs than EDJs, potentially because most of their momentum still comes from the (sub) tropics and is conserved.

For comparison with our earlier categorization method that used only spatial information (longitude, latitude and pressure level of the jet point), we perform the categorization one last time with this choice of discriminant variables. The results can be seen on the fifth and last row of A1, and shows again similar results. This previous method worked well in the North Atlantic basin but was not based on physical bases and did not generalize well to other basins. Both of those concerns are solved with the new method, that can be applied to hemisphere-spanning jets without modification.

Appendix B: Extended jet properties

In the main text, we have highlighted how many jet properties undergo a transition around the month of June, setting this month apart from the rest of ~~summer~~ JJA in terms of absolute values of these jet properties. ~~To explore whether this is also true for the~~

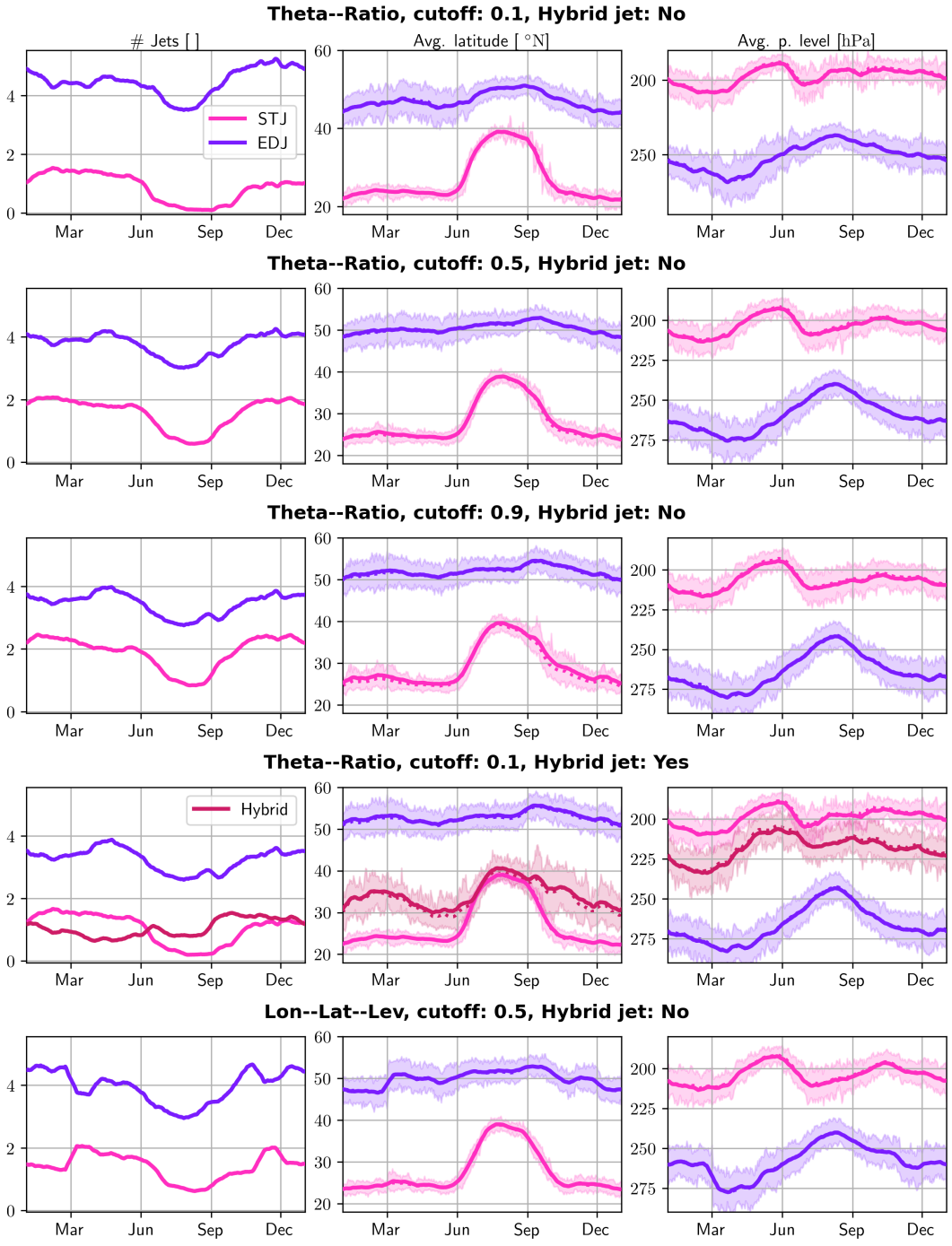

Figure A1. Seasonal variabilities of categorized jet properties with variations in the categorization method.

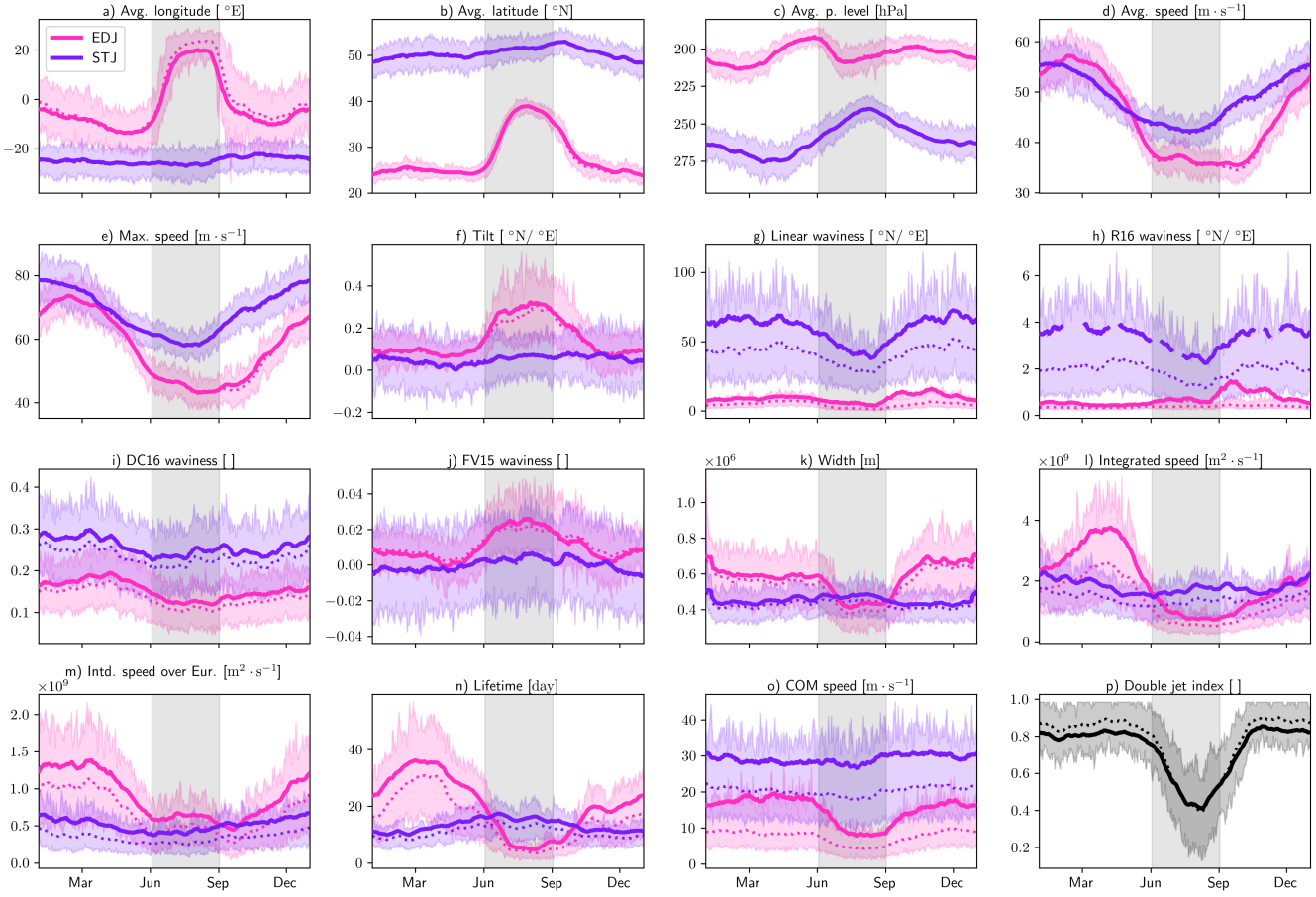

Figure B1. Reproduction of main text's figure 8 with a larger selection of jet properties.

~~trends explored on, e.g., table **??**, we compute, for each calendar day, the yearly trend of each jet property. A 91-day-of-year smoothing is applied to this noisy seasonally-varying trend signal, before it is plotted on Figure B2.~~

~~Reproduction of main text's figure 8 with a larger selection of jet properties.~~

In order to give a more complete overview of the jet properties, we show the seasonal cycle of the complete set on Figure B1~~, as well as the complete set of yearly trends on table **??**~~.

Comparing the jet core's mean and max speeds shows little difference between the two in their seasonal cycles. The max speed trends are ~~epectedly~~ expectedly stronger but they also seem statistically more robust than mean core speed trends. The waviness metrics all show a different seasonal cycle, and even disagree even on which jet category is wavier than the other. Apart from the differences in the original metrics, this discrepancy can also come from how they were adapted to function on ~~jet features~~jets, and more specifically the normalization factor used in several waviness metrics ($1/\Delta\lambda$) that favorises high values for the STJ which is typically much shorter in this domain. Another issue is that ~~several~~ most of these metrics, from

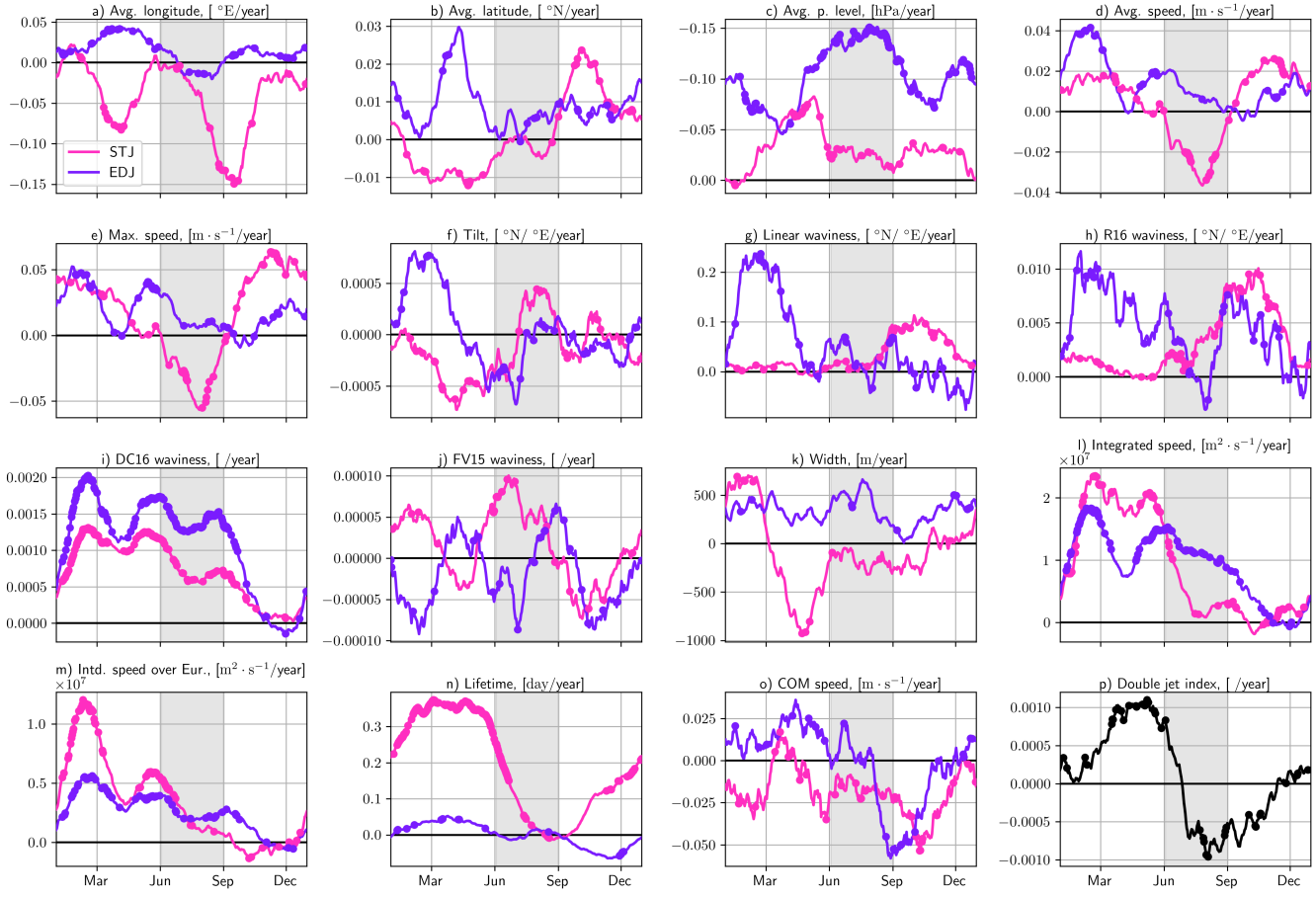

Figure B2. 1959-2022 Day of year ~~yearly~~ inter annual trends, smoothed using ~~91-dayofyear~~ 60-day rolling window averaging. Colored ~~crosses~~ points indicate a significant trend at the 95th percentile.

their definition, ~~treat tilt(1st derivative) the same way they treat curvature (2nd derivative)~~fail to distinguish small synoptic scale waviness and tilt. Only our linear waviness is designed to fully separate the two, but proposing another waviness metric is not our goal with this study. FV15 waviness is very close to our definition of tilt, and the seasonal signals of these two metrics are very similar. ~~Naturally,~~ R16 waviness and linear waviness show an almost identical seasonal cycle too, despite the fact that, from their definitions, on could predict a very different behaviour. Following from our previous comments, it is not surprising that all of the waviness metrics show vastly different trends throughout the year (figure B2).

~~1959- 1979- 1959- 1979- 1959- 1979- 1959- 1979- 1959- 1979- Avg. longitude STJ −24 −50 **−44** −25 14 −20 −6.9 −8.9 −22 −28 [10^{-3} °E/year] EDJ **16** 20 **28** **39** 0.22 −12 −8.2 −23 **8.9** 6.1 Avg. latitude STJ −1.5 1.5 −7.8 −12 −14 −8.2 7.1 **25** **−6.7** 0.32 [10^{-3} °N/year] EDJ 8.8 5.9 11 11 −2.6 6.5 0.8 6.4 4.6 7.4 Avg. p. level STJ −1.8 −3 **−6.8** 2.4 **−7.5** **−8.5** **−5.9** −3.2 **−5.3** −2.5 [10^{-2}hPa/year] EDJ **−7.7** **−9.4** **−9.6** −8.3 **−16** **−20** **−12** **−16** **−11** **−13** Max. speed STJ **3.5**~~

~~2.4 1.9 −2.9 −**3.3** −3.2 **3.4 5.6 2.4** 0.98 [10^{-2}m · s^{-1}/year] EDJ **2.9** 3.8 **2.3 6.6** 1.2 −0.12 **2.8** 1.4 **2.3 2.9** Avg. speed STJ 1.4 0.75 1.2 −2.4 −**2.2** −2 **2.4 4.1 1.4** 0.46 [10^{-2}m · s^{-1}/year] EDJ 1.3 1.2 0.7 **3** 0.63 0.34 0.97 0.12 **0.9** 1.2 Tilt STJ −1.8 −2.4 −**5.2** −0.19 1.8 −1.2 1.6 −4.6 −1.6 −2.3 [10^{-4} °N/ °E/year] EDJ 1.3 −5.2 1.8 −1.9 −2.6 −0.32 −3.3 −5.8 −0.71 −3.3 Linear waviness STJ 5.3 7.1 **10** 3.3 3.9 6.9 −0.82 6.9 **5.3 5.8** [10^{-4} °N/ °E/year] EDJ −0.85 1.9 0.26 1.4 1.1 −3.4 1.9 3.4 0.59 0.84 R16 waviness STJ 2.5 1.5 −3.4 −**14** 9.8 −0.42 12 15 4.2 −0.33 [10^{-4} °N/ °E/year] EDJ 59 85 23 −95 7.3 −79 **78** 36 **42** −14 DC16 waviness STJ 6.5 12 8 14 2.9 14 −3.4 4.6 4.8 11 [10^{-4} /year] EDJ −1.7 2.5 −1.4 3.7 1.6 −3.2 0.18 −2.8 −0.33 0.071 FV15 waviness STJ **4.6** 0.02 −0.1 2.2 6.9 7.5 2.5 3 **2.8** 2.7 [10^{-5} /year] EDJ −2.4 −7.4 1.3 −1.4 0.29 2.8 −**7.2** −**14** −2 −5 Width STJ −**1.8** −1.6 −0.46 −**2.1** −**1.1** −1 −**0.9** −0.33 −**0.84** −**1.2** [10^{3}m/year] EDJ −**0.62** −**1.5** −0.26 −0.43 −0.25 −0.11 −0.36 −0.52 −**0.37** −**0.63** Integrated speed STJ 3.3 5.4 3.7 2.8 −0.63 2.5 0.95 **5** 2.7 4.3 [10^{5}m^{2} · s^{-1}/year] EDJ 1 2.5 0.83 3.6 0.89 −0.87 0.77 −0.88 0.87 1.1 Intd. speed over Eur. STJ 1.1 0.62 −0.01 0.44 0.33 1.1 0.53 **3.1** 0.76 1.4 [10^{5}m^{2} · s^{-1}/year] EDJ **1.1** 1.5 **1.2 2** 0.055 −1 −0.019 −1.1 **0.57** 0.34 Jet lifetime STJ 2.3 −8.9 −5.5 12 −23 15 −7 −4.5 −7.9 2 [10^{-3}day/year] EDJ −0.23 −5.8 1 11 11 13 −1.6 −1.2 2.5 4.3 Speed of COM STJ −14 7.8 20 −4.9 −24 −17 −14 32 −4.3 6.9 [10^{-3}m · s^{-1}/year] EDJ −3.5 7.1 5.9 **23** −11 2.1 −**14** −18 −5.7 4 Double jet index [10^{-4} /year] **5.4** 8.2 **13 21** −3.1 −1.2 −0.74 3.6 **3.6 7.9**~~

Appendix C: Properties of the jets detected on SOM composites

In this Appendix, we validate observations made in the main text about the capacity of SOMs to correctly capture the jet properties. We do so by measuring the properties of the jets detected in the wind field composites of figure 5. The results, shown on figure C1, point towards an overall agreement with some caveats. First, the STJ is not detected in one of the composite, that of cluster 2, even though it is present in some timesteps belonging to this cluster. Wind speed composites also have lower wind speeds than instantaneous fields overall, so the maximum speeds of both jet categories are reduced by about $10\,\mathrm{m.s^{-1}}$. If the absolute values cannot always be meaningfully compared between figures 12 and C1, the distribution of lower and higher values on the SOM can, and in this view there is a large agreement.

Appendix D: Overview of previously tried methods for ~~feature~~ jet core extraction.

During the development of the jet ~~feature~~ core extraction algorithm, several different avenues were explored to improve its robustness or the execution speed and later abandoned in favor of the final version of the algorithm presented in the main text. We believe it is valuable to present negative results, both because these methods could be improved and used again in other relate applications, and simply for future researchers in this field not to try again methods that were explored but ultimately failed at improving the algorithm.

The first version algorithm was an adaptation of the Koch et al. (2006) algorithm, also used in Pena-Ortiz et al. (2013). This algorithm uses a peak finding algorithm on each latitude band, before connecting the points longitudinally based on a distance criterion. The peak finding algorithm requires several thresholds, and their tuning is challenging without an objective quality

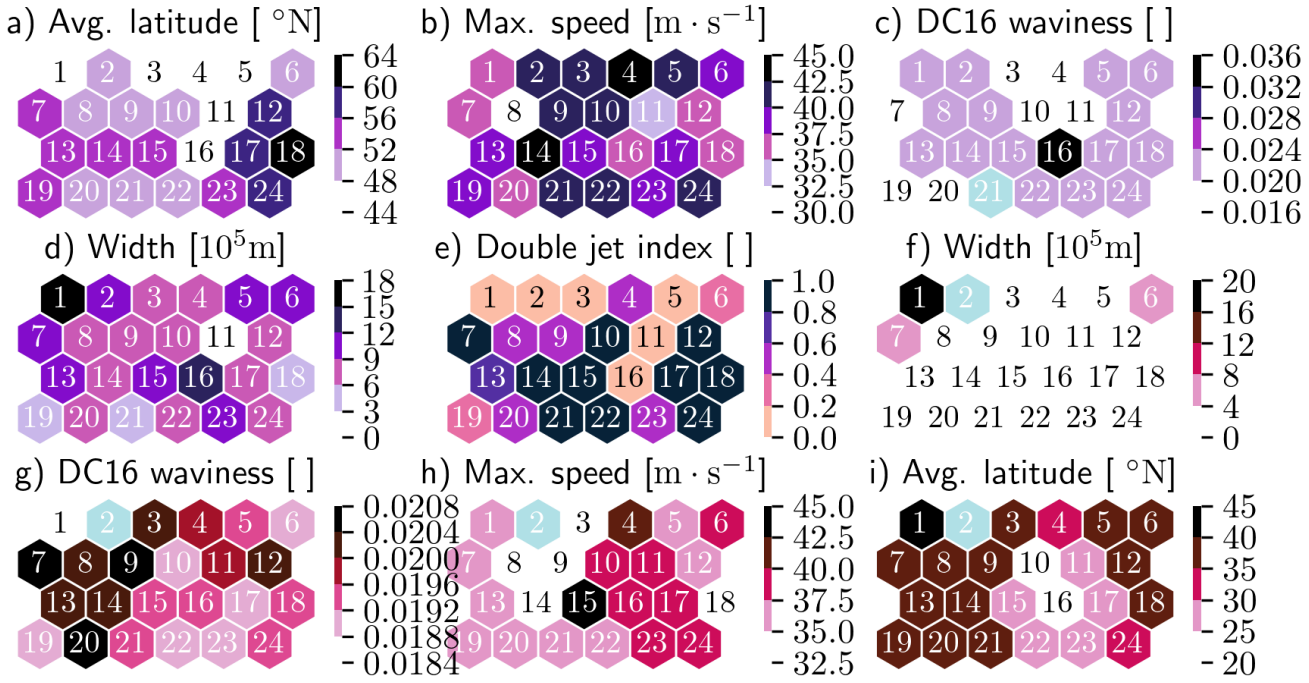

Figure C1. ~~Extended version~~ Jet properties, separated by jet category when applicable, computed from the jets detected on the SOM cluster centers. Shades of ~~table ??~~purple corresponds to EDJ properties and shades of pink to STJ.

metric to grade the performance of the algorithm. More ~~fundamentals problem~~ fundamental problems appear with forked jets, ~~like~~ seen in SOM cluster ~~2~~ 17 for instance.

The second version divides the task in two. First, potential ~~jets~~ jet regions are found using a ~~fairly~~ relatively low wind speed threshold, that can be made seasonally varying or even a quantile threshold to work well in all seasons. The regions are separated from each other using spatial agglomerative clustering. The second step of the algorithm is heavily inspired by Molnos et al. (2017). ~~From potential jets, the jet cores are found using a weighted shortest path algorithm.~~ Each potential jet region is turned into a graph, with each gridpoint a node and edges connecting all of the nodes. The edges are assigned a weight based on the wind speed of the nodes/grid points it connects, and on its alignment with the directional wind field (similar to the current algorithm). From potential jets, the jet cores are found using a weighted shortest path algorithm.

The difficulty of this second method comes from jet regions connecting to each other if they are too close, and the problem of determining start and end points of jet cores within the jet, with potentially several starts and ends within each potential jet region because of the first problem. Several avenues were explored to mitigate the first problem, which in turn made the second problem easier to solve. Most notably, the use of computed vision techniques like thinning, skeletonization and Sato filtering (Sato et al., 1998). This latter technique is used in medical imaging to highlight vessel like structures in black-and-white images like blood vessels in biological tissue, and seems very promising to help in jet detection. However, it also requires

careful setting of its parameters, most crucially its filtering scales which loosely correspond to the expected width of the jet in pixels. Solving these problems made the algorithm grow in complexity and computing requirements for little added benefits. This approach as well as other related ones were finally abandoned in favor of the simpler, more robust one presented in the main text.

Author contributions. OM and TW outlined the study. HB developed the code and performed the study under the supervision of AT, OM and TW. HB wrote the manuscript with contributions and reviews from all co-authors

Competing interests. At least one of the (co-)authors is a member of the editorial board of Weather and Climate Dynamics. The authors have no other competing interests to declare.

Acknowledgements. This work was funded by the Swiss National Science Foundation as part of the project "PERSIST-EUROPE" under grant number 200020_207384.

References

Athanasiadis, P. J., Wallace, J. M., and Wettstein, J. J.: Patterns of Wintertime Jet Stream Variability and Their Relation to the Storm Tracks, https://doi.org/10.1175/2009JAS3270.1, 2010.

Auestad, H., Spensberger, C., Marcheggiani, A., Ceppi, P., Spengler, T., and Woollings, T.: Spatio-Temporal Averaging of Jets Obscures the Reinforcement of Baroclinicity by Latent Heating, Weather and Climate Dynamics, 5, 1269–1286, https://doi.org/10.5194/wcd-5-1269-2024, 2024.

Barnes, E. A. and Hartmann, D. L.: Rossby Wave Scales, Propagation, and the Variability of Eddy-Driven Jets, Journal of the Atmospheric Sciences, 68, 2893–2908, https://doi.org/10.1175/JAS-D-11-039.1, 2011.

Barnes, E. A. and Polvani, L.: Response of the Midlatitude Jets, and of Their Variability, to Increased Greenhouse Gases in the CMIP5 Models, Journal of Climate, 26, 7117–7135, https://doi.org/10.1175/JCLI-D-12-00536.1, 2013.

Barnston, A. G. and Livezey, R. E.: Classification, Seasonality and Persistence of Low-Frequency Atmospheric Circulation Patterns, 1987.

Barriopedro, D., Ayarzagüena, B., García-Burgos, M., and García-Herrera, R.: A Multi-Parametric Perspective of the North Atlantic Eddy-Driven Jet, Climate Dynamics, https://doi.org/10.1007/s00382-022-06574-w, 2022.

Berry, G., Thorncroft, C., and Hewson, T.: African Easterly Waves during 2004—Analysis Using Objective Techniques, Monthly Weather Review, 135, 1251–1267, https://doi.org/10.1175/MWR3343.1, 2007.

Blackport, R. and Fyfe: Climate Models Fail to Capture Strengthening Wintertime North Atlantic Jet and Impacts on Europe, https://doi.org/10.1126/sciadv.abn3112, 2022.

Blackport, R. and Screen, J. A.: Insignificant Effect of Arctic Amplification on the Amplitude of Midlatitude Atmospheric Waves, Science Advances, 6, eaay2880, https://doi.org/10.1126/sciadv.aay2880, 2020a.

Blackport, R. and Screen, J. A.: Weakened Evidence for Mid-Latitude Impacts of Arctic Warming, Nature Climate Change, 10, 1065–1066, https://doi.org/10.1038/s41558-020-00954-y, 2020b.

Bukenberger, M., Rüdisühli, S., and Schemm, S.: Jet Stream Dynamics from a Potential Vorticity Gradient Perspective: The Method and Its Application to a Kilometre-Scale Simulation, Quarterly Journal of the Royal Meteorological Society, 149, 2409–2432, https://doi.org/10.1002/qj.4513, 2023.

Cassou, C., Terray, L., and Phillips, A. S.: Tropical Atlantic Influence on European Heat Waves, Journal of Climate, 18, 2805–2811, https://doi.org/10.1175/JCLI3506.1, 2005.

Cattiaux, J., Peings, Y., Saint-Martin, D., Trou-Kechout, N., and Vavrus, S. J.: Sinuosity of Midlatitude Atmospheric Flow in a Warming World, Geophysical Research Letters, 43, 8259–8268, https://doi.org/10.1002/2016GL070309, 2016.

D'Andrea, F., Duvel, J.-P., Rivière, G., Vautard, R., Cassou, C., Cattiaux, J., Coumou, D., Faranda, D., Happé, T., Jézéquel, A., Ribes, A., and Yiou, P.: Summer Deep Depressions Increase Over the Eastern North Atlantic, Geophysical Research Letters, 51, e2023GL104 435, https://doi.org/10.1029/2023GL104435, 2024.

Davis, N. and Birner, T.: On the Discrepancies in Tropical Belt Expansion between Reanalyses and Climate Models and among Tropical Belt Width Metrics, https://doi.org/10.1175/JCLI-D-16-0371.1, 2017.

Davis, S. M. and Rosenlof, K. H.: A Multidiagnostic Intercomparison of Tropical-Width Time Series Using Reanalyses and Satellite Observations, https://doi.org/10.1175/JCLI-D-11-00127.1, 2012.

Di Capua, G. and Coumou, D.: Changes in Meandering of the Northern Hemisphere Circulation, Environmental Research Letters, 11, 094 028, https://doi.org/10.1088/1748-9326/11/9/094028, 2016.

Dima, I. M. and Wallace, J. M.: On the Seasonality of the Hadley Cell, 2003.

Faranda, D., Messori, G., and Yiou, P.: Dynamical Proxies of North Atlantic Predictability and Extremes, Scientific Reports, 7, 41 278, https://doi.org/10.1038/srep41278, 2017.

Francis, J. A. and Vavrus, S. J.: Evidence Linking Arctic Amplification to Extreme Weather in Mid-Latitudes, Geophysical Research Letters, 39, https://doi.org/10.1029/2012GL051000, 2012.

Francis, J. A. and Vavrus, S. J.: Evidence for a Wavier Jet Stream in Response to Rapid Arctic Warming, Environmental Research Letters, 10, 014 005, https://doi.org/10.1088/1748-9326/10/1/014005, 2015.

Franzke, C. and Woollings, T.: On the Persistence and Predictability Properties of North Atlantic Climate Variability, Journal of Climate, 24, 466–472, https://doi.org/10.1175/2010JCLI3739.1, 2011.

García-Burgos, M., Ayarzagüena, B., Barriopedro, D., and García-Herrera, R.: Jet Configurations Leading to Extreme Winter Temperatures Over Europe, Journal of Geophysical Research: Atmospheres, 128, e2023JD039 304, https://doi.org/10.1029/2023JD039304, 2023.

Geen, R., Thomson, S. I., Screen, J. A., Blackport, R., Lewis, N. T., Mudhar, R., Seviour, W. J. M., and Vallis, G. K.: An Explanation for the Metric Dependence of the Midlatitude Jet-Waviness Change in Response to Polar Warming, Geophysical Research Letters, 50, e2023GL105 132, https://doi.org/10.1029/2023GL105132, 2023.

Gibson, P. B., Perkins-Kirkpatrick, S. E., Uotila, P., Pepler, A. S., and Alexander, L. V.: On the Use of Self-Organizing Maps for Studying Climate Extremes, Journal of Geophysical Research: Atmospheres, 122, 3891–3903, https://doi.org/10.1002/2016JD026256, 2017.

Grams, C. M., Beerli, R., Pfenninger, S., Staffell, I., and Wernli, H.: Balancing Europe's Wind-Power Output through Spatial Deployment Informed by Weather Regimes, Nature Climate Change, 7, 557–562, https://doi.org/10.1038/nclimate3338, 2017.

Hannachi, A., Woollings, T., and Fraedrich, K.: The North Atlantic Jet Stream: A Look at Preferred Positions, Paths and Transitions, Quarterly Journal of the Royal Meteorological Society, 138, 862–877, https://doi.org/10.1002/qj.959, 2012.

Harnik, N., Galanti, E., Martius, O., and Adam, O.: The Anomalous Merging of the African and North Atlantic Jet Streams during the Northern Hemisphere Winter of 2010, Journal of Climate, 27, 7319–7334, https://doi.org/10.1175/JCLI-D-13-00531.1, 2014.

Harnik, N., Garfinkel, C. I., and Lachmy, O.: The Influence of Jet Stream Regime on Extreme Weather Events, in: Dynamics and Predictability of Large-Scale, High-Impact Weather and Climate Events, edited by Li, J., Swinbank, R., Grotjahn, R., and Volkert, H., pp. 79–94, Cambridge University Press, 1 edn., ISBN 978-1-107-77554-1 978-1-107-07142-1 978-1-107-41680-2, https://doi.org/10.1017/CBO9781107775541.007, 2016.

Harvey, B., Hawkins, E., and Sutton, R.: Storylines for Future Changes of the North Atlantic Jet and Associated Impacts on the UK, International Journal of Climatology, 43, 4424–4441, https://doi.org/10.1002/joc.8095, 2023.

Held, I. M.: Momentum Transport by Quasi-Geostrophic Eddies, Journal of the Atmospheric Sciences, 32, 1494–1497, https://doi.org/10.1175/1520-0469(1975)032<1494:MTBQGE>2.0.CO;2, 1975.

Held, I. M.: Large-Scale Dynamics and Global Warming, Bulletin of the American Meteorological Society, 74, 228–242, https://doi.org/10.1175/1520-0477(1993)074<0228:LSDAGW>2.0.CO;2, 1993.

Held, I. M. and Hou, A. Y.: Nonlinear Axially Symmetric Circulations in a Nearly Inviscid Atmosphere, Journal of the Atmospheric Sciences, 37, 515–533, https://doi.org/10.1175/1520-0469(1980)037<0515:NASCIA>2.0.CO;2, 1980.

Hersbach, H., Bell, B., Berrisford, P., Hirahara, S., Horányi, A., Muñoz-Sabater, J., Nicolas, J., Peubey, C., Radu, R., Schepers, D., Simmons, A., Soci, C., Abdalla, S., Abellan, X., Balsamo, G., Bechtold, P., Biavati, G., Bidlot, J., Bonavita, M., De Chiara, G., Dahlgren, P., Dee, D., Diamantakis, M., Dragani, R., Flemming, J., Forbes, R., Fuentes, M., Geer, A., Haimberger, L., Healy, S., Hogan, R. J., Hólm, E., Janisková, M., Keeley, S., Laloyaux, P., Lopez, P., Lupu, C., Radnoti, G., de Rosnay, P., Rozum, I., Vamborg, F., Vil-

laume, S., and Thépaut, J.-N.: The ERA5 Global Reanalysis, Quarterly Journal of the Royal Meteorological Society, 146, 1999–2049, https://doi.org/10.1002/qj.3803, 2020.

Heskes, T.: Energy Functions for Self-Organizing Maps, in: Kohonen Maps, edited by Oja, E. and Kaski, S., pp. 303–315, Elsevier Science B.V., Amsterdam, ISBN 978-0-444-50270-4, https://doi.org/10.1016/B978-044450270-4/50024-3, 1999.

Hochman, A., Messori, G., Quinting, J. F., Pinto, J. G., and Grams, C. M.: Do Atlantic-European Weather Regimes Physically Exist?, Geophysical Research Letters, 48, e2021GL095 574, https://doi.org/10.1029/2021GL095574, 2021.

Hoskins, B. J. and Ambrizzi, T.: Rossby Wave Propagation on a Realistic Longitudinally Varying Flow, 1993.

Hoskins, B. J. and Hodges, K. I.: The Annual Cycle of Northern Hemisphere Storm Tracks. Part I: Seasons, Journal of Climate, 32, 1743–1760, https://doi.org/10.1175/JCLI-D-17-0870.1, 2019.

Huang, C. S. Y. and Nakamura, N.: Local Finite-Amplitude Wave Activity as a Diagnostic of Anomalous Weather Events, Journal of the Atmospheric Sciences, 73, 211–229, https://doi.org/10.1175/JAS-D-15-0194.1, 2016.

Jain, P. and Flannigan, M.: The Relationship between the Polar Jet Stream and Extreme Wildfire Events in North America, Journal of Climate, 34, 6247–6265, https://doi.org/10.1175/JCLI-D-20-0863.1, 2021.

Kållberg, P., Berrisford, P., Hoskins, B., Simmons, A., Uppala, S., Lamy-Thépaut, S., and Hine, R.: ERA-40 Atlas, Tech. Rep. 19, ECMWF, 2005.

Koch, P., Wernli, H., and Davies, H. C.: An Event-Based Jet-Stream Climatology and Typology, International Journal of Climatology, 26, 283–301, https://doi.org/10.1002/joc.1255, 2006.

Kohonen, T.: Self-Organized Formation of Topologically Correct Feature Maps, Biological Cybernetics, 43, 59–69, https://doi.org/10.1007/BF00337288, 1982.

Kohonen, T.: Essentials of the Self-Organizing Map, Neural Networks, 37, 52–65, https://doi.org/10.1016/j.neunet.2012.09.018, 2013.

Krishnamurti, T. N.: The Subtropical Jets Stream of Winter, Journal of the Atmospheric Sciences, 18, 172–191, https://doi.org/10.1175/1520-0469(1961)018<0172:TSJSOW>2.0.CO;2, 1961.

Lachmy, O.: The Relation Between the Latitudinal Shifts of Midlatitude Diabatic Heating, Eddy Heat Flux, and the Eddy-Driven Jet in CMIP6 Models, Journal of Geophysical Research: Atmospheres, 127, https://doi.org/10.1029/2022JD036556, 2022.

Lee, S. and Kim, H.-k.: The Dynamical Relationship between Subtropical and Eddy-Driven Jets, Journal of the Atmospheric Sciences, 60, 1490–1503, https://doi.org/10.1175/1520-0469(2003)060<1490:TDRBSA>2.0.CO;2, 2003.

Lin, L., Hu, C., Wang, B., Wu, R., Wu, Z., Yang, S., Cai, W., Li, P., Xiong, X., and Chen, D.: Atlantic Origin of the Increasing Asian Westerly Jet Interannual Variability, Nature Communications, 15, 2155, https://doi.org/10.1038/s41467-024-46543-x, 2024.

Maddison, J. W., Ayarzagüena, B., Barriopedro, D., and García-Herrera, R.: Added Value of a Multiparametric Eddy-Driven Jet Diagnostic for Understanding European Air Stagnation, Environmental Research Letters, 18, 084 022, https://doi.org/10.1088/1748-9326/ace72e, 2023.

Madonna, E., Li, C., Grams, C. M., and Woollings, T.: The Link between Eddy-Driven Jet Variability and Weather Regimes in the North Atlantic-European Sector, Quarterly Journal of the Royal Meteorological Society, 143, 2960–2972, https://doi.org/10.1002/qj.3155, 2017.

Maher, P., Kelleher, M. E., Sansom, P. G., and Methven, J.: Is the Subtropical Jet Shifting Poleward?, Climate Dynamics, 54, 1741–1759, https://doi.org/10.1007/s00382-019-05084-6, 2020.

Mahlstein, I., Martius, O., Chevalier, C., and Ginsbourger, D.: Changes in the Odds of Extreme Events in the Atlantic Basin Depending on the Position of the Extratropical Jet, Geophysical Research Letters, 39, https://doi.org/10.1029/2012GL053993, 2012.

Martin, J. E.: Recent Trends in the Waviness of the Northern Hemisphere Wintertime Polar and Subtropical Jets, Journal of Geophysical Research: Atmospheres, 126, e2020JD033 668, https://doi.org/10.1029/2020JD033668, 2021.

Martin, J. E. and Norton, T.: Waviness of the Southern Hemisphere Wintertime Polar and Subtropical Jets, Weather and Climate Dynamics, 4, 875–886, https://doi.org/10.5194/wcd-4-875-2023, 2023.

Martius, O.: A Lagrangian Analysis of the Northern Hemisphere Subtropical Jet, https://doi.org/10.1175/JAS-D-13-0329.1, 2014.

Martius, O. and Rivière, G.: Rossby Wave Breaking: Climatology, Interaction with Low-Frequency Climate Variability, and Links to Extreme Weather Events, in: Dynamics and Predictability of Large-Scale, High-Impact Weather and Climate Events, edited by Li, J., Swinbank, R., Grotjahn, R., and Volkert, H., pp. 69–78, Cambridge University Press, 1 edn., ISBN 978-1-107-77554-1 978-1-107-07142-1 978-1-107-41680-2, https://doi.org/10.1017/CBO9781107775541.006, 2016.

Martius, O., Zenklusen, E., Schwierz, C., and Davies, H. C.: Episodes of Alpine Heavy Precipitation with an Overlying Elongated Stratospheric Intrusion: A Climatology, International Journal of Climatology, 26, 1149–1164, https://doi.org/10.1002/joc.1295, 2006.

Martius, O., Schwierz, C., and Davies, H. C.: Tropopause-Level Waveguides, Journal of the Atmospheric Sciences, 67, 866–879, https://doi.org/10.1175/2009JAS2995.1, 2010.

Michel, C. and Rivière, G.: The Link between Rossby Wave Breakings and Weather Regime Transitions, Journal of the Atmospheric Sciences, 68, 1730–1748, https://doi.org/10.1175/2011JAS3635.1, 2011.

Michelangeli, P.-A., Vautard, R., and Legras, B.: Weather Regimes: Recurrence and Quasi Stationarity, Journal of the Atmospheric Sciences, 52, 1237–1256, https://doi.org/10.1175/1520-0469(1995)052<1237:WRRAQS>2.0.CO;2, 1995.

Molnos, S., Mamdouh, T., Petri, S., Nocke, T., Weinkauf, T., and Coumou, D.: A Network-Based Detection Scheme for the Jet Stream Core, Earth System Dynamics, 8, 75–89, https://doi.org/10.5194/esd-8-75-2017, 2017.

Monahan, A. H. and Fyfe, J. C.: On the Nature of Zonal Jet EOFs, https://doi.org/10.1175/JCLI3960.1, 2006.

Nakamura, N. and Huang, C. S. Y.: Atmospheric Blocking as a Traffic Jam in the Jet Stream, Science, 361, 42–47, https://doi.org/10.1126/science.aat0721, 2018.

Osman, M., Beerli, R., Büeler, D., and Grams, C. M.: Multi-Model Assessment of Sub-Seasonal Predictive Skill for Year-Round Atlantic–European Weather Regimes, Quarterly Journal of the Royal Meteorological Society, 149, 2386–2408, https://doi.org/10.1002/qj.4512, 2023.

Palmen, E. and Newton, C. W.: A Study of the Mean Wind and Temperature Distribution in the Vicinity of the Polar Front in Winter, Journal of the Atmospheric Sciences, 5, 220–226, https://doi.org/10.1175/1520-0469(1948)005<0220:ASOTMW>2.0.CO;2, 1948.

Peings, Y., Cattiaux, J., Vavrus, S. J., and Magnusdottir, G.: Projected Squeezing of the Wintertime North-Atlantic Jet, Environmental Research Letters, 13, 074 016, https://doi.org/10.1088/1748-9326/aacc79, 2018.

Pena-Ortiz, C., Gallego, D., Ribera, P., Ordonez, P., and Alvarez-Castro, M. D. C.: Observed Trends in the Global Jet Stream Characteristics during the Second Half of the 20th Century, Journal of Geophysical Research: Atmospheres, 118, 2702–2713, https://doi.org/10.1002/jgrd.50305, 2013.

Röthlisberger, M., Martius, O., and Wernli, H.: An Algorithm for Identifying the Initiation of Synoptic-Scale Rossby Waves on Potential Vorticity Waveguides, Quarterly Journal of the Royal Meteorological Society, 142, 889–900, https://doi.org/10.1002/qj.2690, 2016a.

Röthlisberger, M., Pfahl, S., and Martius, O.: Regional-Scale Jet Waviness Modulates the Occurrence of Midlatitude Weather Extremes: JET WAVINESS AND WEATHER EXTREMES, Geophysical Research Letters, 43, 10,989–10,997, https://doi.org/10.1002/2016GL070944, 2016b.

Rousi, E., Kornhuber, K., Beobide-Arsuaga, G., Luo, F., and Coumou, D.: Accelerated Western European Heatwave Trends Linked to More-Persistent Double Jets over Eurasia, Nature Communications, 13, 3851, https://doi.org/10.1038/s41467-022-31432-y, 2022.

Sato, Y., Nakajima, S., Shiraga, N., Atsumi, H., Yoshida, S., Koller, T., Gerig, G., and Kikinis, R.: Three-Dimensional Multi-Scale Line Filter for Segmentation and Visualization of Curvilinear Structures in Medical Images, Medical Image Analysis, 2, 143–168, https://doi.org/10.1016/s1361-8415(98)80009-1, 1998.

Schneider, E. K.: Axially Symmetric Steady-State Models of the Basic State for Instability and Climate Studies. Part II. Nonlinear Calculations, Journal of the Atmospheric Sciences, 34, 280–296, https://doi.org/10.1175/1520-0469(1977)034<0280:ASSSMO>2.0.CO;2, 1977.

Shaw, T. A. and Miyawaki, O.: Fast Upper-Level Jet Stream Winds Get Faster under Climate Change, Nature Climate Change, 14, 61–67, https://doi.org/10.1038/s41558-023-01884-1, 2024.

Spensberger, C., Spengler, T., and Li, C.: Upper-Tropospheric Jet Axis Detection and Application to the Boreal Winter 2013/14, Monthly Weather Review, 145, 2363–2374, https://doi.org/10.1175/MWR-D-16-0467.1, 2017.

Spensberger, C., Li, C., and Spengler, T.: Linking Instantaneous and Climatological Perspectives on Eddy-Driven and Subtropical Jets, Journal of Climate, 36, 8525–8537, https://doi.org/10.1175/JCLI-D-23-0080.1, 2023.

Stendel, M., Francis, J., White, R., Williams, P. D., and Woollings, T.: The Jet Stream and Climate Change, in: Climate Change, pp. 327–357, Elsevier, ISBN 978-0-12-821575-3, https://doi.org/10.1016/B978-0-12-821575-3.00015-3, 2021.

Stryhal, J. and Plavcová, E.: On Using Self-Organizing Maps and Discretized Sammon Maps to Study Links between Atmospheric Circulation and Weather Extremes, International Journal of Climatology, 43, 2678–2698, https://doi.org/10.1002/joc.7996, 2023.

Totz, S., Petri, S., Lehmann, J., and Coumou, D.: Regional Changes in the Mean Position and Variability of the Tropical Edge, Geophysical Research Letters, 45, 12,076–12,084, https://doi.org/10.1029/2018GL079911, 2018.

Tuel, A. and Martius, O.: Weather Persistence on Sub-Seasonal to Seasonal Timescales: A Methodological Review, Earth System Dynamics, 14, 955–987, https://doi.org/10.5194/esd-14-955-2023, 2023.

Vallis, G. K.: Atmospheric and Oceanic Fluid Dynamics: Fundamentals and Large-Scale Circulation, Cambridge University Press, 2 edn., ISBN 978-1-107-06550-5 978-1-107-58841-7, https://doi.org/10.1017/9781107588417, 2017.

Weiland, R. S., van der Wiel, K., Selten, F., and Coumou, D.: Intransitive Atmosphere Dynamics Leading to Persistent Hot–Dry or Cold–Wet European Summers, Journal of Climate, 34, 6303–6317, https://doi.org/10.1175/JCLI-D-20-0943.1, 2021.

White, R. H.: Time-Varying Atmospheric Waveguides – Climatologies and Connections to Quasi-Stationary Waves, EGUsphere, pp. 1–21, https://doi.org/10.5194/egusphere-2024-966, 2024.

Winters, A. C. and Martin, J. E.: Diagnosis of a North American Polar–Subtropical Jet Superposition Employing Piecewise Potential Vorticity Inversion, Monthly Weather Review, 145, 1853–1873, https://doi.org/10.1175/MWR-D-16-0262.1, 2017.

Winters, A. C., Keyser, D., Bosart, L. F., and Martin, J. E.: Composite Synoptic-Scale Environments Conducive to North American Polar–Subtropical Jet Superposition Events, Monthly Weather Review, 148, 1987–2008, https://doi.org/10.1175/MWR-D-19-0353.1, 2020.

Wirth, V.: Waveguidability of Idealized Midlatitude Jets and the Limitations of Ray Tracing Theory, Weather and Climate Dynamics, 1, 111–125, https://doi.org/10.5194/wcd-1-111-2020, 2020.

Wirth, V. and Polster, C.: The Problem of Diagnosing Jet Waveguidability in the Presence of Large-Amplitude Eddies, Journal of the Atmospheric Sciences, 78, 3137–3151, https://doi.org/10.1175/JAS-D-20-0292.1, 2021.

Woollings, T., Hannachi, A., and Hoskins, B.: Variability of the North Atlantic Eddy-Driven Jet Stream: Variability of the North Atlantic Jet Stream, Quarterly Journal of the Royal Meteorological Society, 136, 856–868, https://doi.org/10.1002/qj.625, 2010.

Woollings, T., Czuchnicki, C., and Franzke, C.: Twentieth Century North Atlantic Jet Variability, Quarterly Journal of the Royal Meteorological Society, 140, 783–791, https://doi.org/10.1002/qj.2197, 2014.

Woollings, T., Barnes, E., Hoskins, B., Kwon, Y.-O., Lee, R. W., Li, C., Madonna, E., McGraw, M., Parker, T., Rodrigues, R., Spensberger, C., and Williams, K.: Daily to Decadal Modulation of Jet Variability, Journal of Climate, 31, 1297–1314, https://doi.org/10.1175/JCLI-D-17-0286.1, 2018a.

Woollings, T., Barriopedro, D., Methven, J., Son, S.-W., Martius, O., Harvey, B., Sillmann, J., Lupo, A. R., and Seneviratne, S.: Blocking and Its Response to Climate Change, Current Climate Change Reports, 4, 287–300, https://doi.org/10.1007/s40641-018-0108-z, 2018b.

Woollings, T., Drouard, M., O'Reilly, C. H., Sexton, D. M. H., and McSweeney, C.: Trends in the Atmospheric Jet Streams Are Emerging in Observations and Could Be Linked to Tropical Warming, Communications Earth & Environment, 4, 1–8, https://doi.org/10.1038/s43247-023-00792-8, 2023.